UNIVERSIDADE DE SÃO PAULO
ESCOLA DE ENGENHARIA DE SÃO CARLOS
DEPARTAMENTO DE ENGENHARIA DE ESTRUTURAS

Fernando Massami Sato

Numerical experiments with stable versions of the Generalized Finite Element Method

São Carlos
2017

FERNANDO MASSAMI SATO

Numerical experiments with stable versions of the Generalized Finite Element Method

CORRECTED VERSION

(Original version is available at EESC-USP)

Dissertation presented to the São Carlos School of Engineering of the University of São Paulo for obtaining the Master degree in Science.

Advisor: Sergio Persival Baroncini Proença

São Carlos

2017

Sato, Fernando Massami
S253n Numerical experiments with stable versions of the Generalized Finite Element Method / Fernando Massami Sato; orientador Sergio Persival Baroncini Proença. São Carlos, 2017.

Dissertação (Mestrado) - Programa de Pós-Graduação em Engenharia Civil(Engenharia de Estruturas) e Área de Concentração em Estruturas -- Escola de Engenharia de São Carlos da Universidade de São Paulo, 2017.

1. Generalized Finite Element Method. 2. Stable Generalized Finite Element Method. 3. Higher Order Generalized Finite Element Method. 4. rate of convergence. 5. scaled condition number. I. Título.

FOLHA DE JULGAMENTO

Candidato: Engenheiro **FERNANDO MASSAMI SATO.**

Título da dissertação: "Experimentos numéricos com versões estáveis do método dos elementos finitos generalizados".

Data da defesa: 21/08/2017.

Comissão Julgadora: **Resultado:**

Prof. Titular **Sergio Persival Baroncini Proença (Orientador)**
(Escola de Engenharia de São Carlos/EESC) APROVADO

Prof. Dr. **Marcos Arndt**
(Universidade Federal do Paraná/UFPR) APROVADO

Prof. Dr. **Leandro Palermo Junior**
(Universidade Estadual de Campinas/UNICAMP) APROVADO

Coordenador do Programa de Pós-Graduação em Engenheira Civil (Engenharia de Estruturas):
Prof. Titular **Humberto Breves Coda**

Presidente da Comissão de Pós-Graduação:
Prof. Associado **Luis Fernando Costa Alberto**

ACKNOWLEDGMENTS

To my advisor, Sergio Proença, for the guidance, patience and friendship during the graduation and master degree research.

To my parents Mauricio and Mary, and my brothers Bruno and Eduardo for the support over the years.

To my grandparents Taro and Kaoru for taking care of me during my childhood.

To my colleagues Dorival and Ayrton for the help during the meetings and programming tips.

To Professor Rodrigo Paccola and Ricardo Angélico for the contributions in my qualification exam.

To CAPES for the financial support.

ABSTRACT

SATO, F. M. **Numerical experiments with stable versions of the Generalized Finite Element Method**. 2017. 97p. Dissertation (Master degree). São Carlos School of Engineering, University of São Paulo, São Carlos, 2017

The Generalized Finite Element Method (GFEM) is essentially a partition of unity based method (PUM) that explores the Partition of Unity (PoU) concept to match a set of functions chosen to efficiently approximate the solution locally. Despite its well-known advantages, the method may present some drawbacks. For instance, increasing the approximation space through enrichment functions may introduce linear dependences in the solving system of equations, as well as the appearance of blending elements. To address the drawbacks pointed out above, some improved versions of the GFEM were developed. The Stable GFEM (SGFEM) is a first version hereby considered in which the GFEM enrichment functions are modified. The Higher Order SGFEM proposes an additional modification for generating the shape functions attached to the enriched patch. This research aims to present and numerically test these new versions recently proposed for the GFEM. In addition to highlighting its main features, some aspects about the numerical integration when using the higher order SGFEM, in particular are also addressed. Hence, a splitting rule of the quadrilateral element area, guided by the PoU definition itself is described in detail. The examples chosen for the numerical experiments consist of 2-D panels that present favorable geometries to explore the advantages of each method. Essentially, singular functions with good properties to approximate the solution near corner points and polynomial functions for approximating smooth solutions are examined. Moreover, a comparison among the conventional FEM and the methods herein described is made taking into consideration the scaled condition number and rates of convergence of the relative errors on displacements. Finally, the numerical experiments show that the Higher Order SGFEM is the more robust and reliable among the versions of the GFEM tested.

Keywords: Generalized Finite Element Method. Stable Generalized Finite Element Method. Higher Order Stable Generalized Finite Element Method. Rate of convergence. Scaled condition number.

RESUMO

SATO, F. M. **Experimentos numéricos com versões estáveis do Método dos Elementos Finitos Generalizados**. 2017. 97p. Dissertação (Mestrado). Escola de Engenharia de São Carlos, Universidade de São Paulo, São Carlos, 2017

O Método dos Elementos Finitos Generalizados (MEFG) é essencialmente baseado no método da partição da unidade, que explora o conceito de partição da unidade para compatibilizar um conjunto de funções escolhidas para localmente aproximar de forma eficiente a solução. Apesar de suas vantagens bem conhecidas, o método pode apresentar algumas desvantagens. Por exemplo, o aumento do espaço de aproximação por meio das funções de enriquecimento pode introduzir dependências lineares no sistema de equações resolvente, assim como o aparecimento de elementos de mistura. Para contornar as desvantagens apontadas acima, algumas versões aprimoradas do MEFG foram desenvolvidas. O MEFG Estável é uma primeira versão aqui considerada na qual as funções de enriquecimento do MEFG são modificadas. O MEFG Estável de ordem superior propõe uma modificação adicional para a geração das funções de forma atreladas ao espaço enriquecido. Esta pesquisa visa apresentar e testar numericamente essas novas versões do MEFG recentemente propostas. Além de destacar suas principais características, alguns aspectos sobre a integração numérica quando usado o MEFG Estável de ordem superior, em particular, são também abordados. Por exemplo, detalha-se uma regra de divisão da área do elemento quadrilateral, guiada pela própria definição de sua partição da unidade. Os exemplos escolhidos para os experimentos numéricos consistem em chapas com geometrias favoráveis para explorar as vantagens de cada método. Essencialmente, examinam-se funções singulares com boas propriedades de aproximar a solução nas vizinhanças de vértices de cantos, bem como funções polinomiais para aproximar soluções suaves. Ademais, uma comparação entre o MEF convencional e os métodos aqui descritos é feita levando-se em consideração o número de condição do sistema escalonado e as razões de convergência do erro relativo em deslocamento. Finalmente, os experimentos numéricos mostram que o MEFG Estável de ordem superior é a mais robusta e confiável entre as versões do MEFG testadas.

Palavras-chave: Método dos Elementos Finitos Generalizados. Método dos Elementos Finitos Generalizados Estável. Método dos Elementos Finitos Generalizados Estável de ordem superior. Razão de convergência. Número de condição escalonado.

LIST OF FIGURES

LIST OF TABLE

LIST OF ABBREVIATIONS

C-XFEM	Corrected eXtended Finite Element Method
DoF	Degrees of Freedom
FEM	Finite Element Method
GFEM	Generalized Finite Element Method
PoU	Partition of Unity
PUM	Partition of Unity Method
SCIEnCE	São Carlos Integrity Environment for Computational Engineering
SCN	Scaled Condition Number
SGFEM	Stable Generalized Finite Element Method

LIST OF SYMBOLS

ϕ_{α}^{j}	Shape function
φ_{α}	Partition of unity
$L_{(\alpha)}^{j}$	Enrichment function
$\hat{u}_{\alpha}$	Conventional degree of freedom
$\tilde{u}_{(\alpha)}^{j}$	Additional nodal parameter
$L_{\alpha}^{\mathrm{j\ (mod)}}$	Modified enrichment function
$I_{\omega_{\alpha}}$	Interpolant function of nodal values
$\phi_{\alpha}^{\mathrm{j\ (mod)}}$	Modified shape function
S_{FEM}	Standard FEM approximation space
$S_{enrich}^{\mathrm{mod}}$	Augmented space related to the modified enrichment functions
φ_{α}^{FT}	Flat-top partition of unity
σ	Parameter for controlling the flat region length that can vary between 0.0 and 0.5
γ	Angle for the singular function measured internally to the solid
n_{singular}	Number of terms optionally adopted for singular function

CONTENTS

1 INTRODUCTION

The Finite Element Method (FEM) is indeed one of the most powerful tools of computational engineering. However, this method has shown to be ineffective or having limited efficacy when used to simulate problems presenting some special features, such as solids containing reentrant corners, cracks, materials interfaces and boundary layers. In fact, to account for these kinds of features, an exaggerated mesh refinement is normally required around these singularity regions. Therefore, using conventional FEM, obtaining satisfactory numerical results demands higher computational costs.

The Generalized Finite Element Method (GFEM), Strouboulis, Babuška and Copps (2000), was proposed both to address the mesh refinement problem and efficiently solve the above mentioned classes of special problems, therefore overcoming some of the inconveniences presented by the FEM.

The GFEM is essentially a partition of unity based method (PUM) that explores the Partition of Unity (PoU) concept to match a set of functions chosen to efficiently approximate the solution locally. These local approximations are called enrichment functions and once matched increase the global conforming approximation space.

The GFEM contains the FEM shape functions in particular. However, differently from the standard FEM, where the shape functions are attached to elements, in the GFEM the shape functions are attached to a node. This node is vertex of a local patch, which is the region where the shape function is defined. In the GFEM, overlapping patches covering the domain of the problem can be defined with the help of a finite element mesh. A patch is then defined by the set of elements sharing a common node, which is its vertex.

The main characteristic of the GFEM is the possibility to introduce an a priori knowledge into the approximation about the solution through the enrichment functions. Moreover, according to the peculiarities of the problem, the method enables the selective improvement of the approximation space only where it is necessary. Consequently, a good global approximate solution can be obtained even if using a coarse mesh, therefore reducing the computational cost.

Despite the above mentioned advantages, the method may present some drawbacks. For instance, increasing the approximation space through enrichment functions may result in a system of equations linearly dependent. In this case, round-off errors prevail when solving the system, making the approximate solution less reliable. As will be shown later, the level of instability can be assessed by the Scaled Condition Number (SCN). In the worst cases of instability, the SCN is of a higher order of magnitude compared to the FEM level. Another drawback presented by the GFEM derives from the so-called blending elements. This kind of element appears when the enrichment is limited to a restricted region of the domain or number of patches. Then, looking at the elements of a mesh, instead of the patches, it may happen that only some nodes are enriched or that the nodes show a different number of enrichment functions. Consequently, unwanted approximation terms appear, adversely influencing the rate of convergence of the global solution.

To address the drawbacks mentioned above, some improved versions of the GFEM were developed, such as the Stable Generalized Finite Element Method (SGFEM), Babuška and Banerjee (2012) and the Corrected eXtended Finite Element Method (C-XFEM), Fries (2008). In this research, the C-XFEM will not be considered.

The SGFEM is a version of the GFEM where the enrichment functions are modified. In short, the modified enrichment function is the enrichment function of the GFEM minus a linear or bilinear interpolation of its nodal values. This version was proposed with the premise of solving two issues: the linear dependency of the resulting system and the unwanted terms existing in the blending elements.

Despite its premise, the SGFEM can still be ineffective for solving the problem of linear dependences, as exemplified by the examples presented herein. In fact, when considering complete second degree enrichment, for instance, the SCN is shown to be likewise bad, once presenting a magnitude order comparable to the value obtained for GFEM. To deal with this issue, a new improved 2-D GFEM version called Higher Order SGFEM, Zhang, Banerjee and Babuška (2014), is also introduced and hereby tested.

The Higher Order SGFEM proposes a further modification for generating the shape functions attached to the enriched patch. This improvement consists of using a flat-top PoU for multiplying the local enrichment functions. Due to the particular features of the flat-top PoU, it is expected that

the resulting set of shape functions is linearly independent. In fact, the effectiveness of this improved version of the GFEM is numerically demonstrated in the examples hereby presented.

1.1 Objectives

The main aim is to present and test some of the new developments recently proposed for the GFEM. In particular, an improved formulation of the method called Stable GFEM, as well as its higher order version are addressed through a numerical investigation.

As the main objective, the purpose of this research is to compare the above mentioned GFEM versions with the conventional FEM. The focus is to identify the advantages and shortcomings of each method, and to conclude if there is one among them which is more robust and reliable.

1.2 Materials and methods

The methodology adopted in this research consists firstly of a bibliographic review about the GFEM and its improved versions, SGFEM and higher order SGFEM.

The second step comprises an investigation of the advantages and shortcomings of each method through two-dimensional numerical examples. The analysis was conducted using the São Carlos Integrity Environment for Computational Engineering (SCIEnCE) code, which has already had these versions implemented.

Moreover, the analysis of the numerical results was then taken as a guideline for proceeding the investigation. For instance, based on the results it was shown that when considering a complete polynomial as enrichment, both GFEM and SGFEM reveal high scaled condition numbers, therefore indicating ill-conditioning of the resulting system of equations. To overcome this disadvantage, a 2-D version of the higher order SGFEM was implemented and tested.

Finally, a comparison between the methods herein described and the conventional FEM is made through selected numerical examples. For instance, the rates of convergence for the relative errors

on displacements and the scaled condition number were used to highlight the overall GFEM efficacy and also to identify which one among the GFEM versions is more robust and reliable.

1.3 Structure of the dissertation

Besides the Introduction section, this dissertation has seven more chapters. The outline of the chapters is as follows:

In Chapter 2, a brief review of the GFEM is presented. However, some details are given regarding the formulation, main advantages and drawbacks of the method. Moreover, the modified versions developed to overcome the GFEM drawbacks are addressed.

Chapter 3 is related to the SGFEM. Essentially, the modification of the enrichment function, aiming to overcome the GFEM problems is emphasized.

In Chapter 4, the Higher Order version of the SGFEM is presented. The main aspects related to the flat-top PoU definition for 1-D and 2-D analysis using quadrilateral elements are discussed, including some comments on the numerical integration.

Chapter 5 focuses on the numerical integration of the resulting 2-D enriched shape functions for the Higher Order SGFEM. In particular, a splitting rule of the quadrilateral element area, guided by the PoU definition itself is described in detail.

In Chapter 6, the enrichment functions considered in this research are presented. Essentially, singular functions with good properties to approximate the solution near corner points and the polynomial functions for approximating smooth solutions are examined.

In Chapter 7, three numerical examples are presented. The first one is an L-shaped panel, in which the reentrant corner favors the use of a special enrichment. The second example is a panel containing an edge crack. Again, enrichments with special and polynomial functions are explored. The third example is an irregular polygonal panel containing multiple voids and reentrant corners, as well as two edge cracks. In these examples, comparisons among the GFEM versions are made in relation to the h-convergence rate and scaled condition number.

In Chapter8, the conclusions and final remarks are presented.

2 THE GENERALIZED FINITE ELEMENT METHOD

The generalized finite element method was developed to solve problems where the standard FEM is inefficient or is costly computationally due to the extreme mesh refinement required, e.g. problems involving stress concentrations induced by cracks and reentrant corners, boundary layers and materials interfaces. The main idea of this method is to increase the FEM trial and test function spaces with functions *a priori* in harmony with the solution.

2.1 A brief historical review

The GFEM can be seen as a version of Galerkin's method, which is characterized by the availability of more flexible approximations to the solutions of boundary value problems.

Historically, the conception of this method is preceded by the seminal proposal of Babuška and Osborn (1983), according to which the shape of the approximation function is ruled by the differential equation of its own problem. Next, Babuška, Caloz and Osborn (1994) proposed the Special Finite Element Method. In this version, local approaches presenting characteristics of the solution sought were incorporated into the approximation space using the Partition of Unity (PoU) concept. Later, the idea of exploring the PoU for matching the local approximations and constructing a global approximation was formalized in the Partition of Unity Method (PUM), Melenk and Babuška (1996).

The PUM is a new finite element method that can create conform approximation spaces presenting local features that are interesting for the solution. One of the main advantages of this method is that an *a priori* knowledge of the solution can be incorporated into the approximation space. Moreover, approximation spaces with any regularity can be easily constructed.

The construction of the approximation space of the PUM essentially explores the concepts of Partition of Unity and covering sets called patches or clouds. Accordingly, the domain Ω of the given problem is covered by overlapping subdomains Ω_i. A set of enrichment functions associated to each subdomain is then defined as: $L_i = \left\{ L_j^{(i)} \,\middle|\, L_j^{(i)} \subset H^1\left(\Omega_i\right) \right\}$, where H^1 is the Hilbert space of

functions with continuous first order derivative. The global approximation to the solution can then be defined as

$$u_{PUM} = \sum_i \phi_i \left(\sum_j u_j^{(i)} L_j^{(i)} \right) \tag{1}$$

where $L_j^{(i)}$ is the enrichment function, $u_j^{(i)}$ parameter involved in the linear combination of the enrichment functions and the sequence of shape functions ϕ_i are a partition of unity C^0 which is used to paste together the local enrichments, thus ensuring continuity for the global approximation.

In GFEM, the shape functions are defined in subdomains called patches. The concept of patches was preceded by the concept of clouds introduced by Duarte (1996) in its proposition of the hp-Cloud method. A patch in the GFEM is a subdomain created, for example, by quadrilateral elements sharing a common node called vertex V_i. In each patch, the functions ϕ_i that appear in the relation (1) show the unity value at the vertex of this subdomain and the null value on its boundary.

Moreover, as shown in Figure 1(a), the shape functions ϕ_i are constructed by gathering the PoU of each element τ_i and attaching them to the vertex of the patch, defined as follows:

$$\varphi_k^{(i)} = \frac{(1+\xi_k \xi)(1+\eta_k \eta)}{4} \tag{2}$$

Figure 1 – (a) Representation of the pyramid or hat basis function ϕ_i for a patch formed by quadrilateral elements and vertex V_i. (b) Master element.

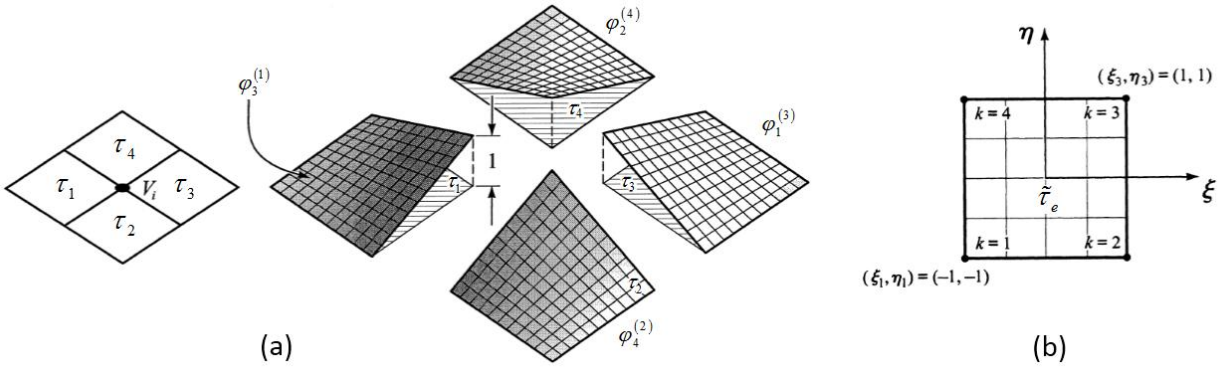

Adapted: Strouboulis, Babuška and Copps (2000)

In the relation (2), the superscript *i* is for the element in the patch, *k* is the node number of the element in coincidence with the vertex, while ξ and η are the coordinates of the master quadrilateral element shown in Figure 1(b).

Finally, once the partition of unity $\varphi_k^{(i)}$ merge, the resulting function ϕ_i is piecewise bilinear. The PoU generated by the overlapping of subdomains is C^0 and will guarantee the inter-element continuity and will create a C^0 approximation.

As the main advantages of the GFEM, the following can be mentioned:

a) for each patch, a set of enrichment functions can be adopted presenting characteristics of good local approximation for the solution;
b) through the concept of the augmented trial space of the FEM, a better approximated solution can be obtained without the need of exploring a refined mesh;
c) there is a possibility of using meshes which are independent of the domain geometry, as depicted in Figure 2, however by doing this two meshes need to be created. One approximation mesh and an integration mesh, Figures 2(a) and 2(b), respectively.

Figure 2 – Example of an independent geometry domain mesh. (a) The approximation mesh that contains the integration mesh. (b) The integration mesh. (c) and (d) details of the integration mesh.

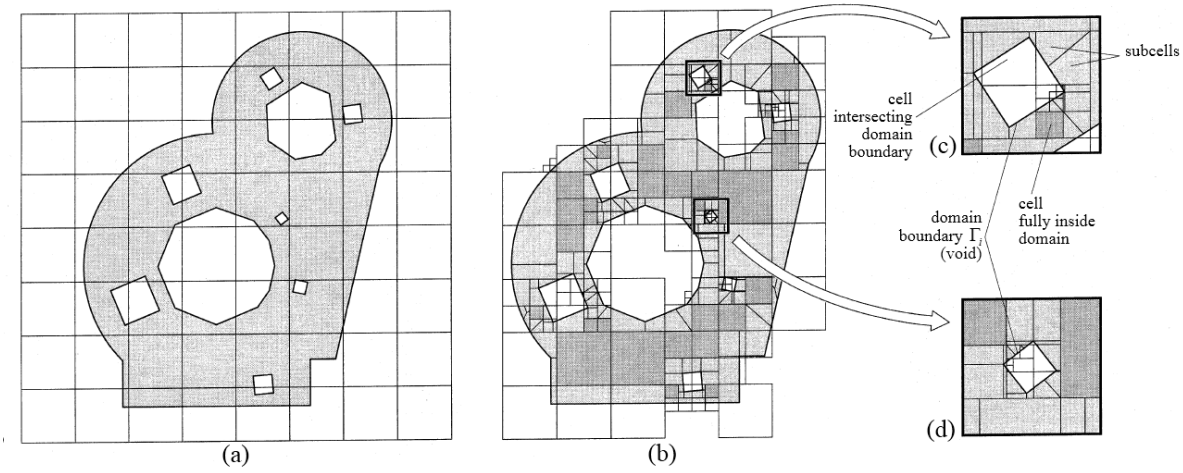

Adapted: Strouboulis, Copps and Babuška (2001)

Despite the possibility of using a mesh independent of the domain, this research explores the standard non-overlapping FEM meshes, e.g. the mesh is built by subdividing the domain into

triangular or quadrilateral elements satisfying the restrictions about the connections between the neighbor elements, as shown in Figure 3.

Figure 3 – Type of mesh used in this research

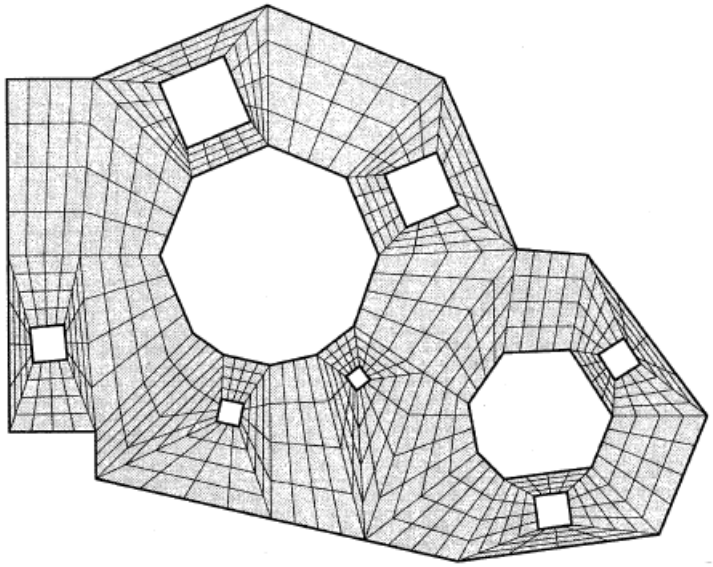

Adapted: Strouboulis, Copps and Babuška (2001)

Therefore, considering a standard FEM mesh, as well as exploring the concepts of PUM and local enrichments in the patches, the formulation of the GFEM is formally presented next.

2.2 Formulation

Despite exploring a mesh of elements, the shape functions of GFEM are conceptually different from those of the conventional FEM, as their construction follows the PUM framework. In fact, in the GFEM the shape functions are attached to patches ω_α, while in the FEM the shape functions are defined in finite elements.

Therefore, the GFEM shape functions (ϕ_α^j) result from the multiplication among the linear or bilinear partition of unity (φ_α) provided by triangular and quadrilateral elements, respectively, and

the enrichment functions ($L^j_{(\alpha)}$), functions that contain the *a priori* knowledge of the solution. This construction process is illustrated in Figure 4.

$$\phi^j_\alpha = \varphi_\alpha \cdot L^j_{(\alpha)} \tag{3}$$

Figure 4 – Construction of the shape function of GFEM using as enrichment (a) polynomial (b) non-polynomial functions. Where φ_α is the hat partition of unity, $L^j_{(\alpha)}$ the enrichment function and ϕ^j_α the shape function of GFEM.

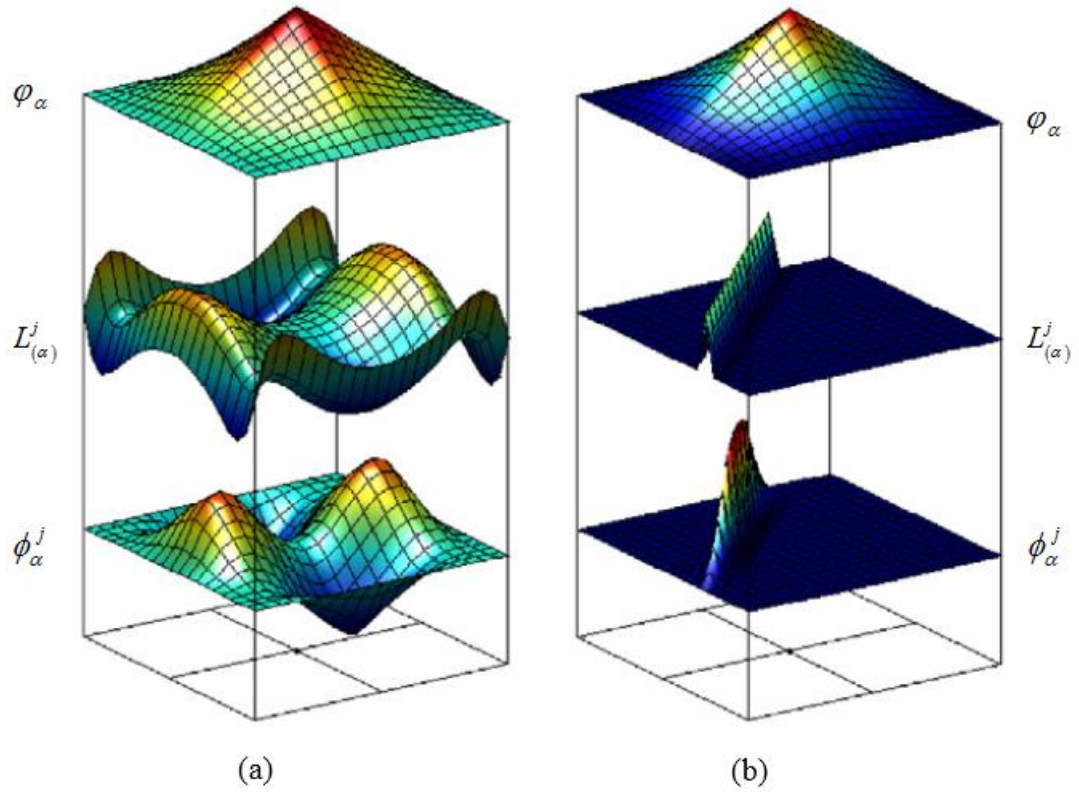

Adapted: Gupta, Kim and Duarte (2012)

In relation (3), $j = 1,\ldots,m(\alpha)$ where $m(\alpha)$ is the number of components of the enrichment vector basis ($L_{(\alpha)}$), which can be different from patch to patch.

Conventionally, the first component of the enrichment vector basis is the unity. Therefore, considering a discretization with N nodes covering the problem domain and adopting an enrichment vector for each of them, the global approximation field for the solution of a boundary value problem can be expressed as follows:

$$
\begin{aligned}
u_h &= \sum_{\alpha=1}^{N} \sum_{j=1}^{m(\alpha)} \varphi_{\alpha}^{j} \tilde{u}_{(\alpha)}^{j} \\
&= \sum_{\alpha=1}^{N} \phi_{\alpha}(x) \hat{u}_{\alpha} + \sum_{\alpha=1}^{N_e} \phi_{\alpha}(x) \left[\sum_{j=2}^{m(\alpha)} L_{(\alpha)}^{j}(x)\ \tilde{u}_{(\alpha)}^{j} \right] \\
&= \sum_{\alpha=1}^{N} \phi_{\alpha}(x) \hat{u}_{\alpha} + \sum_{\alpha=1}^{N_e} \phi_{\alpha}(x) \tilde{L}_{\alpha}
\end{aligned}
\qquad \text{(4a,b,c)}
$$

In the relation (4b), N_e $(\leq N)$ is the number of enriched nodes. The first sum refers to an approximation given by the PoU multiplied by the unity, i.e. this sum refers to the standard FEM approximation, and involves conventional degrees of freedom ($\hat{u}_{\alpha}$) attached to the nodes of the finite element. The second sum involves additional nodal parameters $\tilde{u}_{(\alpha)}^{j}$, associated to the remaining components of the enrichment vector basis. Moreover, the sum between brackets at relation (4b) can be condensed into the parameter $\tilde{L}_{\alpha}$ that contains the enrichment functions and the additional nodal parameters for each node α. The relation (4c) shows the role of the PoU for matching the local approximations.

As already mentioned before, the enrichment functions provide local approximations. Moreover, as exemplified in relation (4), the enrichment is not necessarily imposed for the whole set of nodes, i.e., a number of nodes can remain having the unity as its single component in the enrichment vector basis. This possibility of selective enrichment can be useful, for instance, in domains presenting reentrant corners and/or cracks. In fact, in this kind of problem, the solution can be smooth in most of the domain, however presenting some sort of singularity only in the neighborhood of the crack or reentrant corner.

The local approximation provided by the method is a key advantage indeed, however there may be drawbacks. When selective enrichment is adopted, at the element level, no enriched elements, uniformly enriched elements or blending elements, in this case presenting different levels of enrichment in their nodes, can appear. Consequently, the approximation of the blending element in particular can be badly affected and special treatment is needed in these elements for recovering its effectiveness.

2.3 Some general comments on the Blending Elements

Considering a given mesh, as a result of the selective local enrichment, the elements can be collected in three distinctive categories. The first one includes the standard elements that do not present enriched nodes. In the second category are the so-called reproducing elements that have all the nodes with the same enrichment functions. The third one comprises the blending elements that only have some of their nodes enriched or have different enrichments at the nodes. In the second category, as a consequence of the PoU sum property equal to one, the enrichment function can be reproduced precisely inside the elements. The lack of this favorable feature is the main drawback of the blending elements. Therefore, in the last category, the enrichment functions cannot be reproduced and depending on the type of function, the resulting local approximation can affect directly both the quality of the global approximation and rate of convergence. The element classification mentioned is illustrated in Figure 5.

Figure 5 – Element type classification

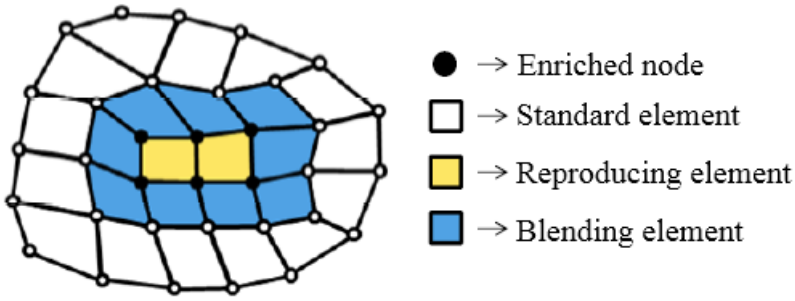

Adapted: Lins (2015)

Still regarding blending elements, according to Fries (2008) the issue requiring the most attention is the introduction of unwanted terms in the approximation due to the difference among nodal enrichments. The uneven or unwanted terms cannot be reproduced inside the element and impact the convergence rate significantly. In the following example, a quadrilateral element containing only one node enriched is considered:

$$u_h = \sum_{\alpha=1}^{N} \varphi_\alpha(x)\hat{u}_\alpha + \varphi_{\bar{\alpha}}(x) L^2_{\bar{\alpha}}(x)\tilde{u}^2_{\bar{\alpha}} \tag{5}$$

where N is the number of nodes and $\bar{\alpha}$ is the enriched node. In general, the application of enrichment functions produces unwanted terms that result from $\varphi_{\bar{\alpha}}(x)L_{\bar{\alpha}}^2$ and its detrimental influence cannot be compensated by the FEM part $\sum_{\alpha=1}^{N}\varphi_\alpha(x)\hat{u}_\alpha$. Therefore, the only way to not generate unwanted terms is making $\tilde{u}_{\bar{\alpha}}^2 = 0$, which means that the enrichment is deactivated.

To overcome the drawbacks caused by the blending elements, some new versions of the GFEM have been proposed. Some of them are briefly specified below:

a) Stable Generalized Finite Element Method (SGFEM): this method proposes a modification in the enrichment functions that can reduce the deleterious influence of blending elements on the rate of convergence, Babuška and Banerjee (2012);
b) Corrected eXtended Finite Element Method (C-XFEM): this method introduces a ramp function on the blending elements to eliminate unwanted terms of approximation and to recover the property of reproducibility of the enrichment, Fries (2008);
c) C^k-GFEM: This method explores PoU with higher regularity build by the moving least square technique, Torres, Barcellos and Mendonça (2015).

The SGFEM was chosen in this research for treating the blending elements because this method was conceived to overcome not only the blending element effects, but also the additional drawback associated to the ill-conditioning of the stiffness matrix.

2.4 On the conditioning of the underlying linear system

Essentially, the conditioning of a linear system of equations is related to how reliable the solution will be.

Consider the linear system $Ax = c$. If the system is well-conditioned, it means that a small change in the coefficient matrix A or a small change in vector c will result in a small change in the solution vector x. On the other hand, if the system is ill-conditioned, a small change in matrix A or a small change in vector c will result in a significant change in solution vector x.

The condition number is a scalar measure of the conditioning of a system and, therefore, indicates the loss of accuracy of the computed solution. If the condition number is small then the system is well conditioned, otherwise, it is ill conditioned. An ill-conditioned matrix includes linear dependencies among its equations.

In the GFEM, as any function can be used as enrichment, the underlying linear system may not be well conditioned with respect to the mesh and enrichment adopted. This shortcoming occurs when functions presenting similar characteristics are adopted, such as PoU and enrichment. For instance, when hat functions are adopted as PoU and polynomial are used for enrichment, the shape functions may result almost linearly dependent and, therefore, the stiffness matrix is ill conditioned.

Regarding its measure, a condition number close to the value computed for the FEM is an acceptable indicator of well conditioning of the GFEM underlying the linear system. Here, a further improved measure called Scaled Condition Number (SCN) of the stiffness matrix will be used, Babuška and Banerjee (2012). According to Zhang, Banerjee and Babuška (2014), given the coefficient matrix A, this value can be obtained by computing the condition number $\kappa_2(\cdot)$ of the scaled matrix $\hat{A}$ based on $\|\cdot\|_2$ vector norm, as indicated below:

$$k(A) := \kappa_2\left(\hat{A}\right) = \kappa_2\left(DAD\right) = \left\|\hat{A}\right\|_2 \left\|\hat{A}^{-1}\right\|_2 \tag{6}$$

where D is a diagonal matrix having its diagonal terms computed as: $D_{ii} = A_{ii}^{-1/2}$.

In this equation, the scaled matrix $\hat{A}$ is obtained by pre and post multiplying the coefficient matrix A by the diagonal matrix D. Moreover, the SCN can also be calculated by the ratio between the largest and smallest eigenvalues of the scaled matrix.

A way to reduce the occurrence of linear dependencies in the GFEM is to use enrichment functions that are of a different nature with respect to the PoU. In other words, if the PoU is polynomial, a non-polynomial enrichment function should be used.

However, even if the dependencies are presented and consequently the SCN is large, it is possible to solve a linear system where the stiffness matrix is semi-positive definite. It can be done by making a scaling process on the stiffness matrix and after that, imposing a little perturbation in its diagonal terms, as originally proposed by Strouboulis, Babuška and Copps (2000). It is important

to note that although the ill-conditioned system can deliver multiple solutions to the unknown coefficients, the boundary value problem presents a unique solution.

The above mentioned procedure for solving the ill-conditioned system is iterative hence, depending on the problem it can be computationally costly. Therefore, the SGFEM was conceived as a more robust and general method to avoid the problem of the ill-conditioned stiffness matrix.

3 THE STABLE GENERALIZED FINITE ELEMENT METHOD

The so-called Stable Generalized Finite Element Method is a new version developed to overcome two drawbacks observed in the GFEM. The method does not have the ill conditioning problem of the stiffness matrix and significantly reduces the negative effects caused by blending elements, Babuška and Banerjee (2012).

The basic difference between the stable and the conventional versions of the GFEM is a simple modification in the enrichment functions used to obtain the shape functions. In SGFEM, the enrichment function is modified in such a way that its values at the patch nodes are equal to zero. The construction of this modified enrichment function $\left(L_\alpha^{\mathrm{j\ (mod)}}\right)$ is shown below:

$$L_\alpha^{\mathrm{j\ (mod)}} = L_\alpha^j - I_{\omega_\alpha}\left(L_\alpha^j\right) \tag{7}$$

where $I_{\omega_\alpha}\left(L_\alpha^j\right)$ is the linear or bilinear piecewise interpolant of nodal values of the enrichment function L_α^j for the patch ω_α. Therefore, I_{ω_α} is:

$$I_{\omega_\alpha} = \sum_{i=1}^{N_{ep}} \varphi_i L_\alpha^j\left(x_i, y_i\right) \tag{8}$$

Where N_{ep} is the number of element nodes belonging to the patch, i is the node of the element in analysis and $\left(x_i, y_i\right)$ is its coordinates.

Once the enrichment functions are modified, the SGFEM shape functions can be constructed similarly to the GFEM:

$$\phi_\alpha^{\mathrm{j\ (mod)}} = \varphi_\alpha \cdot L_\alpha^{\mathrm{j\ (mod)}} \tag{9}$$

Figure 6 illustrates the construction of the SGFEM nodal shape function.

Figure 6 – Construction of SGFEM shape function

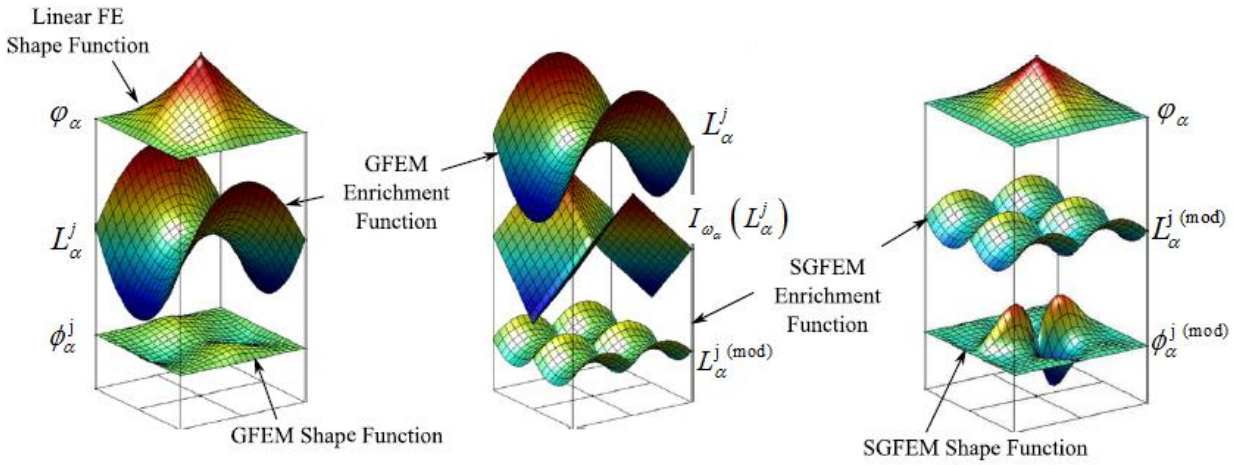

Adapted: Gupta et al. (2015)

As the vector of enrichment functions presents the unity as its first component, the approximation space to the field of interest can be split as in GFEM:

$$u_h = S_{FEM} + S_{enrich}^{\mathrm{mod}} \tag{10}$$

where S_{FEM} is the standard FEM approximation space and $S_{enrich}^{\mathrm{mod}}$ is the augmented space related to the modified enrichment functions. Since the construction of the shape functions and therefore the approximated field for SGFEM is the same as for GFEM, this method is easy to implement.

Concerning the issue of the blending elements, since the values of the SGFEM shape functions are null at the element nodes, the effects of unwanted terms in the approximation are reduced. Therefore, no special treatment in the blending elements is necessary.

As can be concluded from the procedure mentioned above, the modification of the enrichment function basically eliminates the linear portion of it, therefore avoiding conflict with the linear approximation ability already presented in the PoU. Consequently, the equations of the system are expected to be better conditioned and the scaled condition number close to that obtained for FEM. Even though such good features are actually verified in the 1-D approach, the scaled condition number for SGFEM could still be large in the 2-D approach, as demonstrated by the examples described herein. To overcome this problem, a further modification to the method can be implemented leading to the higher order version of the Stable GFEM, hereby selected to be studied and implemented in the SCIEnCE code.

4 THE HIGHER ORDER SGFEM

The higher order SGFEM, Zhang, Banerjee and Babuška (2014), was developed to yield higher order convergence and to ensure good conditioning of the stiffness matrix in any dimensional approach. This new version of the GFEM is derived from a further specific modification of the enrichment space aiming to ensure that the shape functions of the enriched space are locally almost linearly independent, while maintaining good flexibility for the construction of local approximations as in the standard SGFEM.

Essentially, the suggested modification consists of using another PoU for constructing the S_{enrich}^{mod} space, different from the piecewise hat functions that however are preserved for constructing the basic S_{FEM} space. Thus, the higher order SGFEM approximation space is represented as follows:

$$S_{SGFEM} = S_{FEM} + S_{enrich}^{\text{mod}} \tag{11}$$

$$\begin{aligned} S_{FEM} &= \sum_{\alpha=1}^{N} \varphi_\alpha u_\alpha^1 \\ S_{enrich}^{\text{mod}} &= \sum_{\alpha=1}^{N_e} \varphi_\alpha^{FT} \sum_{j=2}^{N_L(\alpha)} L_\alpha^{j\,(\text{mod})} a_\alpha^j \end{aligned} \tag{12}$$

In the S_{enrich}^{mod} space definition, $L_{\alpha i}^{\text{mod}}$ is constructed as indicated in relation (7), where $N_L(\alpha)$ is the number of enrichment functions applied on node α, while φ_α^{FT} represents the so-called 'flat-top' PoU function, Griebel and Schweitzer (2002). According to Zhang, Banerjee and Babuška (2014), the use of another partition of unity to construct the S_{enrich}^{mod} will contribute to generating linearly independent enrichment spaces, and consequently, a good conditioning of the linear system will be warranted.

$$\varphi_{Left}^{FT}(x)=\begin{cases}1 & x\in\left[x_j,\,x_j+\sigma h\right]\\ \left(1-\left(\dfrac{x-x_j-\sigma h}{(1-2\sigma)h}\right)^{l}\right)^{l} & x\in\left[x_j+\sigma h,\,x_j+(1-\sigma)h\right]\\ 0 & x\in\left[x_j+(1-\sigma)h,\,x_{j+1}\right]\end{cases} \tag{13}$$

$$\varphi_{Right}^{FT}(x)=\begin{cases}0 & x\in\left[x_j,\,x_j+\sigma h\right]\\ 1-\left(1-\left(\dfrac{x-x_j-\sigma h}{(1-2\sigma)h}\right)^{l}\right)^{l} & x\in\left[x_j+\sigma h,\,x_j+(1-\sigma)h\right]\\ 1 & x\in\left[x_j+(1-\sigma)h,\,x_{j+1}\right]\end{cases} \tag{14}$$

The relations defining the flat-top PoU attached to a two node bar element and hereby adopted in the 1-D approach are presented below. The relations above $\varphi_{Left}^{FT}(x)$ and $\varphi_{Right}^{FT}(x)$ are for the functions attached to the left and to the right node, respectively, x_j and x_{j+1} are the nodal coordinates, *h* is the element length, σ is a parameter for controlling the flat region length that can vary between 0 and 0.5 and *l* is a positive integer for controlling the smoothness of the curve segment linking the flat regions. Figure 7 (a) and (b) shows, respectively, the functions $\varphi_{Left}^{FT}(x)$ and $\varphi_{Right}^{FT}(x)$ for a 1-D master element in correspondence to $h=2$, $\sigma=0.25$ and $l=1$.

Figure 7 – Representation of flat-top partition of unity. (a) 1-D function for the left node, (b) 1-D function for the right node

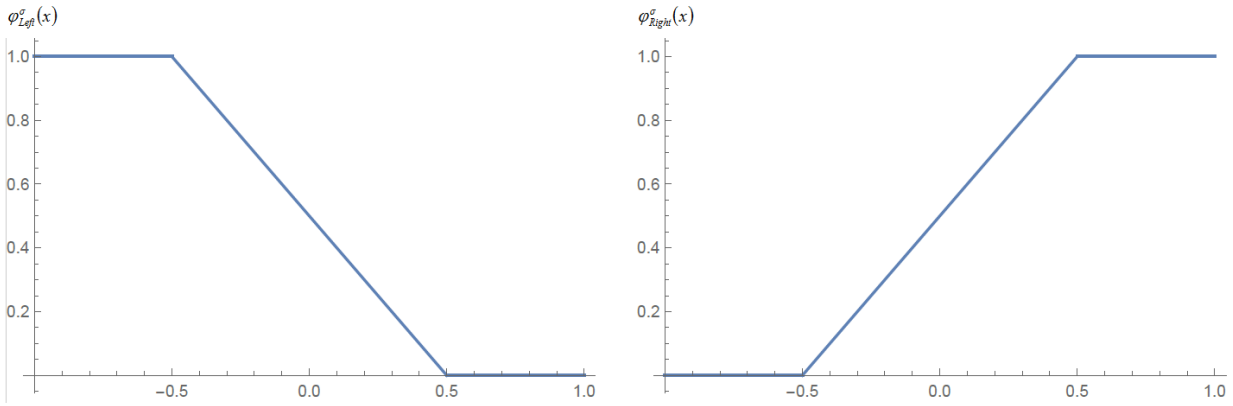

The tensorial product of the 1-D functions described above is used for constructing the 2-D version of the flat-top PoU associated to a regular quadrilateral element depicted in Figure 8.

Figure 8 – Quadrilateral element

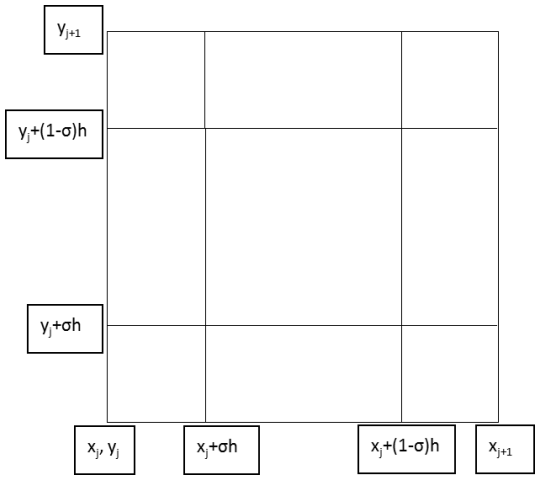

The relations defining the component attached to node 1 are the following.

$$\varphi_1^{FT} = 1 \qquad \text{for} \quad \begin{matrix} x \in \left(x_j, x_j + \sigma h \right) \\ y \in \left(y_j, y_j + \sigma h \right) \end{matrix}$$

$$\varphi_1^{FT} = \left(1 - \left(\frac{x - x_j - \sigma h}{(1-2\sigma)h} \right)^l \right)^l \left(1 - \left(\frac{y - y_j - \sigma h}{(1-2\sigma)h} \right)^l \right)^l \quad \text{for} \quad \begin{matrix} x \in \left[x_j + \sigma h, x_j + (1-\sigma)h \right] \\ y \in \left[y_j + \sigma h, y_j + (1-\sigma)h \right] \end{matrix}$$

$$\varphi_1^{FT} = 0 \qquad \text{for} \quad \begin{matrix} x \in \left(x_j + (1-\sigma)h,\, x_{j+1} \right) \\ y \in \left(y_j, y_{j+1} \right) \end{matrix}$$

$$\varphi_1^{FT} = 0 \qquad \text{for} \quad \begin{matrix} x \in \left(x_j, x_j + (1-\sigma)h \right) \\ y \in \left(y_j + (1-\sigma)h,\, y_{j+1} \right) \end{matrix}$$

$$\varphi_1^{FT} = \left(1 - \left(\frac{x - x_j - \sigma h}{(1-2\sigma)h} \right)^l \right)^l \qquad \text{for} \quad \begin{matrix} x \in \left[x_j + \sigma h, x_j + (1-\sigma)h \right] \\ y \in \left[y_j, y_j + \sigma h \right] \end{matrix}$$

$$\varphi_1^{FT} = \left(1 - \left(\frac{y - y_j - \sigma h}{(1-2\sigma)h} \right)^l \right)^l \qquad \text{for} \quad \begin{matrix} x \in \left[x_j,\, x_j + \sigma h \right] \\ y \in \left[y_j + \sigma h, y_j + (1-\sigma)h \right] \end{matrix}$$

The relations to the remaining nodes are quite similar. The resulting flat-top function attached to node 1 of the quadrilateral master element is depicted in Figure 9 (a) and (b) in correspondence to $h = 2$, $\sigma = 0.25$ and $l = 1$.

Figure 9 – Representation of flat-top PoU 2D version

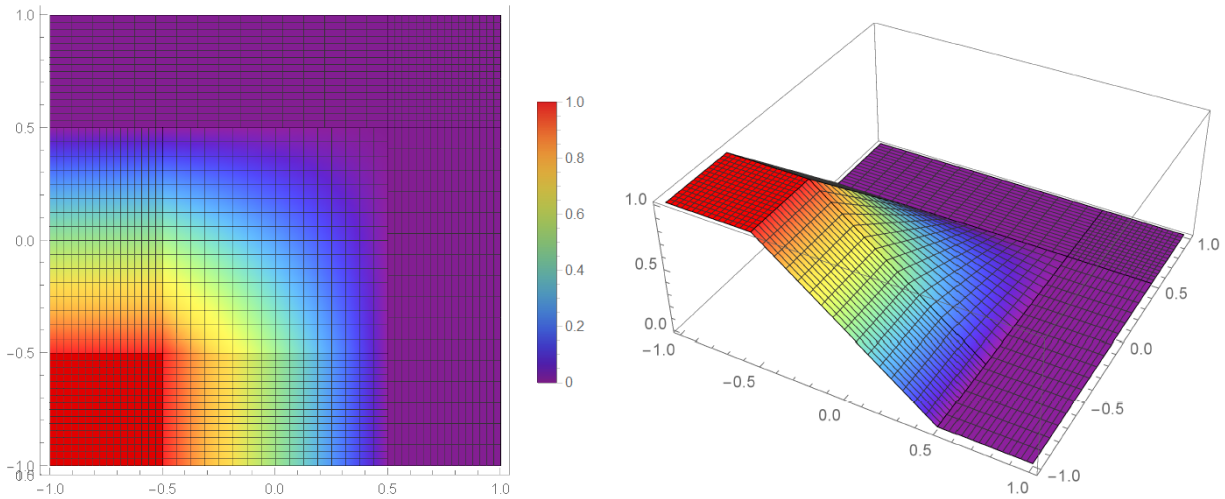

(a) (b)

When the flat-top partition of unity is used, caution should be taken regarding the numerical integration either of the stiffness matrix or the equivalent nodal force vector.

For instance, considering a four node quadrilateral element, if the conventional Gauss-Legendre quadrature rule is assumed for the numerical integration, it is necessary to pay attention to the number of integration points that will be adopted. In fact, despite a number of 3x3 integration points being enough for integrating a bilinear portion of the PoU, it may generate an erroneous result if the flat-top PoU is the function to be integrated. Moreover, as shown before, the geometry of the flat-top depends on the value of the parameter σ. As an example, consider the case where three conventional integration points are adopted, as illustrated in Figure 10.

Figure 10 – Illustration of flat-top PoU with $\sigma = 0.1$ and three integration points (black dots in the figure)

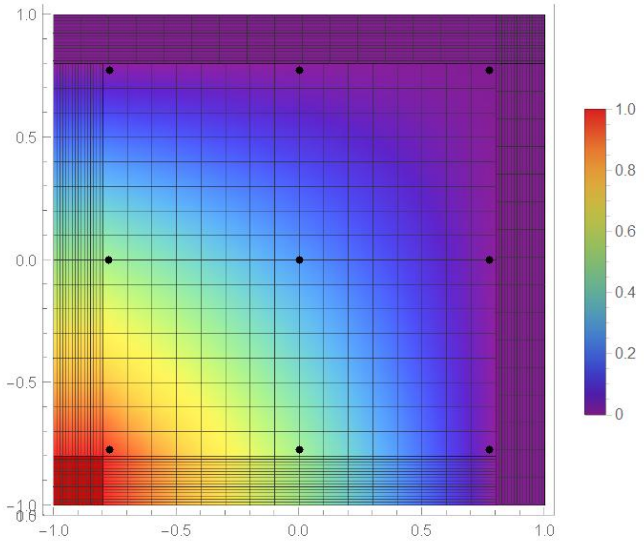

If the aim is to integrate a flat-top relative to $\sigma = 0.1$, only the bilinear portion of the function receives the integration points and consequently the approximated value of the element integral is affected.

The strategy herein adopted for improving numerical integrations through the quadrature rule is presented next.

5 NUMERICAL INTEGRATION AND SPLIT STRATEGY FOR HIGHER ORDER SGFEM

The Gauss-Legendre quadrature rule is applied to numerically integrate both the element stiffness matrix and the element equivalent nodal force vector components when the flat-top PoU described herein is involved.

As well known, the Gaussian quadrature is efficient if the function to be integrated can be well approximated by a polynomial function. However, this may not be the case in the GFEM when special functions are used for enrichment. Therefore, the Gaussian quadrature may not return a good result in such situations. Even so, the rule is hereby considered by using a great number of integration points whenever necessary.

As mentioned, for the case of flat-top PoU, a different strategy for the numerical integration is adopted to avoid the inconvenience caused by the relation number of integration points and value of σ.

Four characteristics of the flat-top PoU component can be revealed when considering the master element domain, as shown in Figure 11(a), each one expressed by a polynomial function.

Figure 11 – Split in subdomains for flat-top PoU.

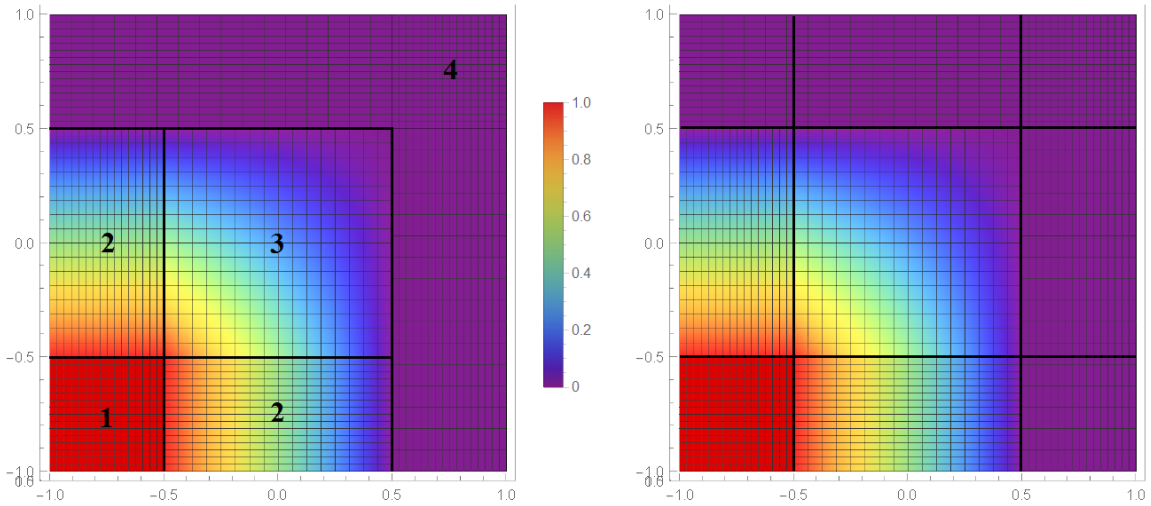

(a) (b)

Areas 1 and 4 have constant values 1 and 0 respectively, areas 2 are described by a ‘ramp’ function and area 3 is described by a higher order polynomial function.

Therefore, the element can be split into nine parts, as shown in Figure 11(b), next applying the Gauss quadrature rule to each subdomain for computing the components of the stiffness matrix and equivalent nodal force vector. Moreover, the numerical integration encompasses only regions 1 to 3. Essentially, this is the strategy hereby adopted for generating the results of the examples presented later on.

6 THE ENRICHMENT FUNCTIONS

Two types of enrichment functions are hereby considered aiming to assess if the SGFEM can effectively overcome the ill-conditioned issue. The first type is the singular function and is suggested to deal with problems with reentrant corners and cracks. The second type is the polynomial function, whose effectiveness is known in problems where the expected solution is smooth. The main features of these enrichments are presented next.

6.1 Singular function

The singular function is used to better describe the stress distribution in a close vicinity of a corner. According to Szabo and Babuška (1991), the exact solution of 2-D problems presenting corners in their geometry identified by a finite number of points can be given by a sum of two functions: one smooth function u_1 and another one u_2 that takes into account the singularities in the corners' vicinity. Function u_2 in polar coordinates is expressed by:

$$u_2 = \sum_{i=1}^{M_k} A_i \cdot r^{\lambda_i} \cdot \psi_i(\theta) \tag{15}$$

Where M_k is the number of corner points, r and θ are local coordinates, A_i are coefficients that depend on the loading, $\psi_i(\theta)$ are smooth functions and λ_i is a parameter related to the singularity.

In view of the general feature of the singular functions shown in relation (15), the enrichment function hereby adopted is written as:

$$L_{\alpha(k)} = r^{\lambda_k} \cdot f_k(\theta) \tag{16}$$

It is worth observing that this function is the solution to the Laplace's problem (which can be specialized to plane linear elasticity or thermal analysis, for example), defined in a domain Ω presenting at its edge corners characterized by an angle γ measured internally to the solid, as shown

in Figure 12. In each corner, the singular solution can be expressed by a series, as presented in the next relation:

Figure 12 – Example of a problem containing a reentrant corner.

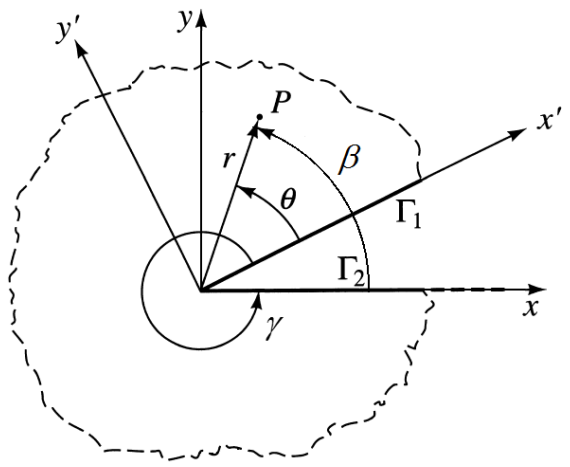

Adapted: Strouboulis, Babuška and Copps (2000)

$$u = \sum_{k=1}^{n_{\text{singular}}} a_k \cdot r^{\lambda_k} \cdot f_k(\theta) \tag{17}$$

$$f_k(\theta) = \begin{cases} \cos(\lambda_k \theta) & \text{if } \Gamma_1 \text{ and/or } \Gamma_2 \text{ have Neumann boundary condition} \\ \sin(\lambda_k \theta) & \text{if } \Gamma_1 \text{ and/or } \Gamma_2 \text{ have Dirichlet boundary condition} \end{cases} \tag{18}$$

$$\lambda_k = \begin{cases} \dfrac{k\pi}{\gamma} & \text{if } \Gamma_1 \text{ and } \Gamma_2 \text{ have both Neumann or both Dirichlet} \\ \dfrac{(2k-1)\pi}{2\gamma} & \text{if } \Gamma_1 \text{ and } \Gamma_2 \text{ have mixed boundary conditions} \end{cases} \tag{19}$$

In relation (17), n_{singular} is the number of terms optionally adopted. Figure 13 depicts the representation of Equation (17) considering Γ_1 and Γ_2 both Dirichlet boundaries and k varying from 1 to 3.

Figure 13 – Illustration of Equation (16) for Γ_1 and Γ_2 both Dirichlet boundaries. (a) k = 1. (b) k = 2. (c) k = 3.

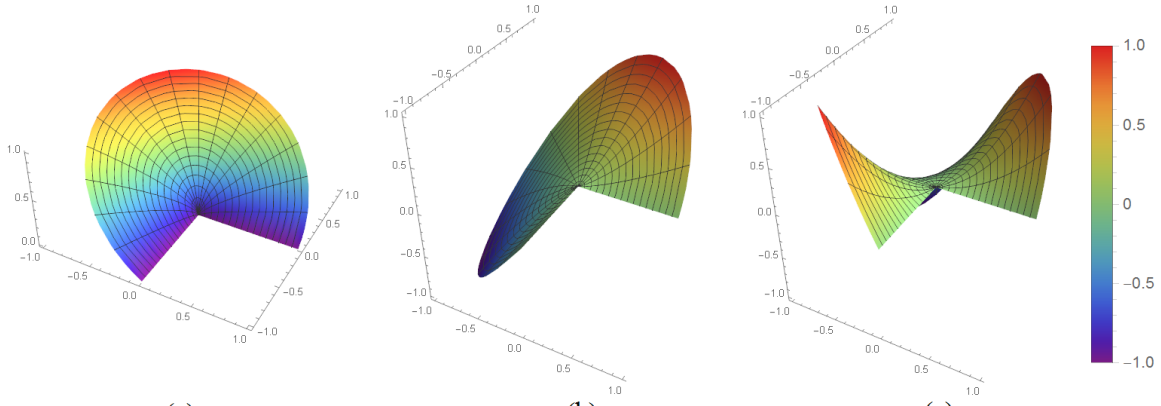

(a) (b) (c)

As will be shown later, for the problems discussed in this work, the number of terms has little influence on the relative displacements, therefore n_{singular} = 1 will be adopted.

Moreover, it is important to observe that stress concentration occurs only for a certain range of the internal angle γ. Since the stress depends on the first derivatives of the function, Relation (16) represents a stress concentration when its first derivatives goes to infinity when the radius goes to zero, otherwise this relation acts as a sine or cosine function and does not return a stress concentration at the corner. Table 1 shows the first derivative for the singular function of the four possible combinations of boundary conditions.

Table 1 – First derivative for the singular function

	Situation 1	Situation 2	Situation 3	Situation 4
Γ_1	Dirichlet	Dirichlet	Neumann	Neumann
Γ_2	Dirichlet	Neumann	Neumann	Dirichlet
L	$r^{\lambda}\cdot\sin(\lambda\theta)$	$r^{\lambda}\cdot\sin(\lambda\theta)$	$r^{\lambda}\cdot\cos(\lambda\theta)$	$r^{\lambda}\cdot\cos(\lambda\theta)$
λ	π/γ	$\pi/2\gamma$	π/γ	$\pi/2\gamma$
$\partial L/\partial x$	$\lambda r^{\lambda-1}\cdot\sin(\lambda\theta-\beta)$	$\lambda r^{\lambda-1}\cdot\sin(\lambda\theta-\beta)$	$\lambda r^{\lambda-1}\cdot\cos(\lambda\theta-\beta)$	$\lambda r^{\lambda-1}\cdot\cos(\lambda\theta-\beta)$
$\partial L/\partial y$	$\lambda r^{\lambda-1}\cdot\cos(\lambda\theta-\beta)$	$\lambda r^{\lambda-1}\cdot\cos(\lambda\theta-\beta)$	$\lambda r^{\lambda-1}\cdot\sin(\beta-\lambda\theta)$	$\lambda r^{\lambda-1}\cdot\sin(\beta-\lambda\theta)$

In the equation above, β is the angle between the x-axis and the point in analysis, Figure 12.

Since the values of sine and cosine are in the range of $[-1,1]$ the first derivatives will tend to go towards infinity only if $r^{\lambda-1} \to \infty$. For situations 1 and 3, where the boundary conditions are both Dirichlet or both Neumann, this occurs for $\pi < \gamma \leq 2\pi$ which results in a $\lambda < 1$. For situations 2 and 4 where mixed boundary conditions are applied, this occurs for $\pi/2 < \gamma \leq 2\pi$.

6.2 Polynomial functions

Polynomial functions have a smooth behavior. The general form of the polynomial enrichment component basis can be expressed by the shifted arrangement as follows:

$$L(m,n) = \frac{(x - x_\alpha)^m (y - y_\alpha)^n}{h^{m+n}} \tag{20}$$

Where x_α and y_α are the coordinates of the patch with vertex node α and h is a scaling factor given, for instance, by the radius of the circle centered at the vertex and circumscribing the largest element of the patch.

One advantage of the shifted enrichment functions is that they are zero in the node where they are imposed. It follows that the physical meaning of the original degree of freedom associated to the basic part of the approximation at such a node is preserved. Moreover, this feature enables one, in principle, to directly enforce displacement boundary conditions in the same way as in the FEM.

In this work, two possibilities of polynomial enrichments will be tested. The first one is a complete quadratic polynomial that contains the set: $(m=1;n=1),(m=2;n=0),(m=0;n=2)$. The second one is the incomplete quadratic polynomial, i.e., the first set without the mixed term, therefore: $(m=2;n=0),\ (m=0;n=2)$.

7 NUMERICAL EXAMPLES AND DISCUSSION

Three examples consisting of 2-D panels of unitary thickness were hereby selected to illustrate in particular the performance of the SGFEM with flat-top PoU for constructing the approximations to the solutions. Plane stress conditions were assumed in all of the examples. Structured meshes were adopted and a combination of shifted polynomial with singular function explored as enrichments. Moreover, the material was supposed to present the linear elastic response and a Young's Modulus with a reference value of 100.0 and a Poisson's ratio of 0.3 were adopted for the elastic parameters.

The first example is an L-shaped panel. The basic aim is to analyze both the convergence order and the scaled condition number provided by the combined effects of mesh refinement and nodal enrichments. In addition, the good characteristics and shortcomings of each of these explored resources are also observed.

The second example has the purpose of showing that the methods are quite efficient even if a crack is presented at the edge of a rectangular panel.

In the last example, the overall potential of the GFEM versions hereby considered is illustrated. Therefore, a complex panel with external polygonal geometry containing multiple reentrant corners, internal large voids and edge cracks is tested.

7.1 L-shaped panel

This example consists of an L-shaped panel under uniform distributed loading at the longer edges. Sliding supports are prescribed at the Dirichlet boundary condition and corner points, as depicted in Figure 14. Furthermore, Dirichlet boundary conditions are imposed using a penalization technique.

Six structured meshes varying from coarse to fine and composed by bilinear quadrilateral elements were used to analyse the h-convergence, however for the study of the SCN, only the four coarser meshes were considered due to the loss of accuracy for the finer meshes. These meshes are

indicated according to the number of elements defined respectively in the longer and shorter edges as: 4x2, 8x4, 16x8, 32x16, 64x32 and 128x64.

Figure 14 – L-shaped panel

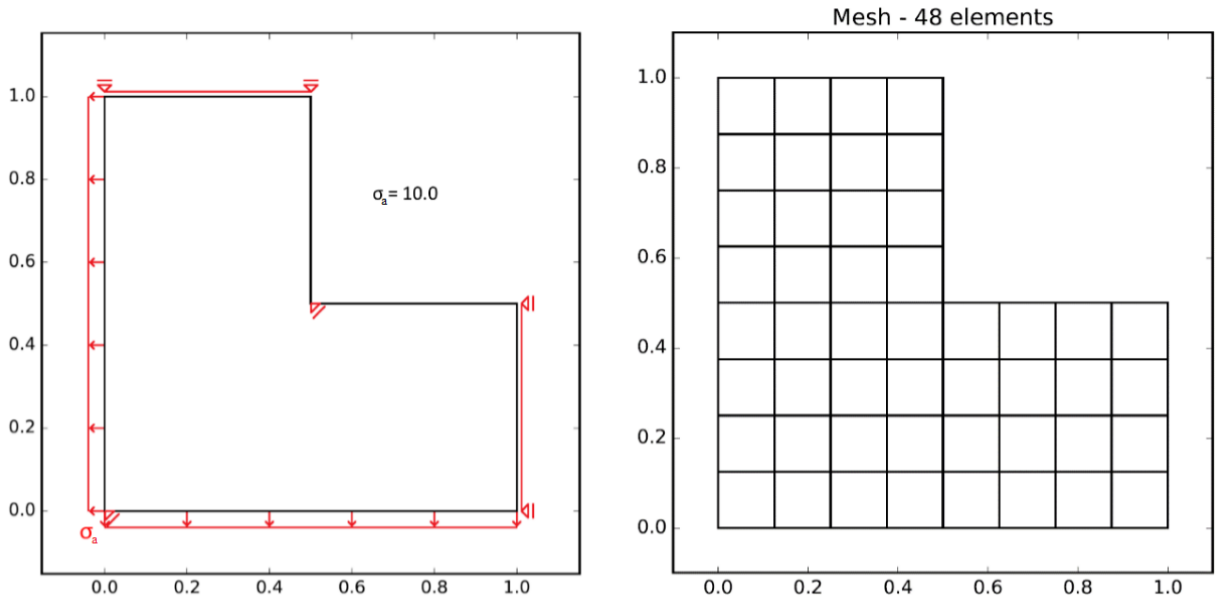

Moreover, the problem is analysed through GFEM versions under four different conditions:

a) In the first one, a study about the σ parameter of the flat-top PoU is made;

b) In the second condition, only the polynomial enrichment is applied. The basic aim is to carefully observe the shortcoming introduced by the linear dependencies associated to this kind of enrichment. Therefore, the large scaled condition number of each version of the method is highlighted;

c) In the third condition only the singular enrichment is applied and the effect of the blending elements is observed;

d) In the fourth condition, both enrichments above are applied. The aim is to show that the versions of the method can provide good approximate solutions even if a course mesh is used.

7.1.1 σ Parameter analysis

As shown before, the parameter σ of the flat-top partition of unity controls the lengths of the flat portions of the function. In particular, taking $\sigma = 0$, the hat-function PoU is recovered and taking $\sigma = 0.5$, the Heaviside step function is recovered (presenting values 1 or 0 in the domain).

Since the split strategy of numerical integration described in topic 5 is adopted for the higher order SGFEM, values for σ between limits 0 and 0.5, as well the number of integration points can be chosen arbitrarily. Therefore, a study considering different values of σ is hereby made seeking to verify its efficacy.

The analysis of the results is presented next by comparing the convergence rates of the relative errors in the displacement for σ equal to 0.01, 0.1, 0.2, 0.3 and 0.4. Moreover, the complete quadratic polynomial is considered as enrichment.

Using the ℓ_2 norm, the relative error on displacements is defined as follows:

$$\text{relative error} = \frac{\left\| u_{ref} - \tilde{u} \right\|_{\ell_2}}{\left\| u_{ref} \right\|_{\ell_2}} \tag{21}$$

In the relation above, u_{ref} is for the reference solution computed by FEM using a very refined structured mesh (2048x1024) and ũ is for the approximate solution. The h-convergence curves in a log x log graphs are presented in Figure 15.

Figure 15 – L-shaped panel: h-convergence for different values of σ

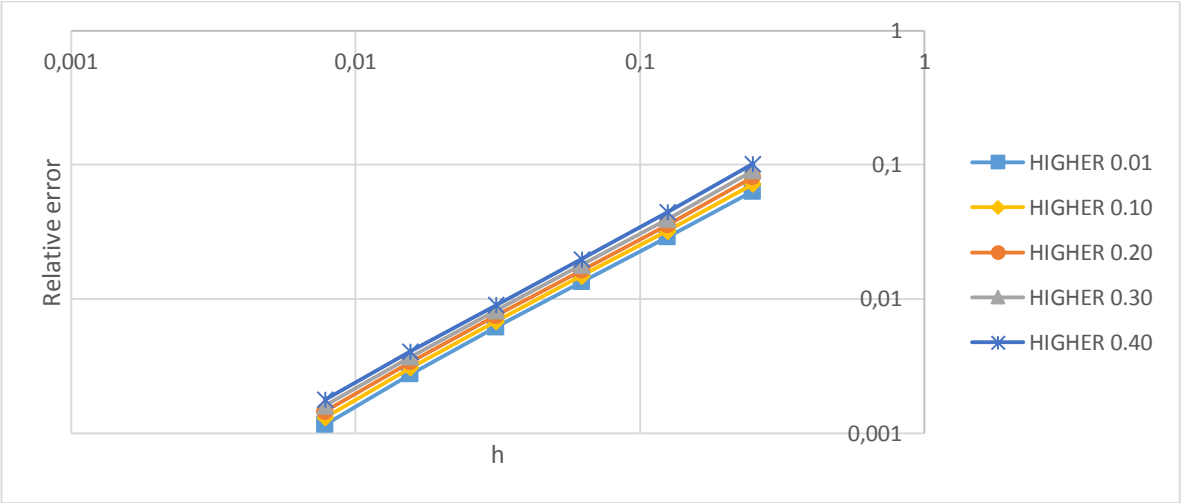

It can be concluded that the lower the σ value is, the better the solution becomes. In fact, by decreasing the σ value, the flat-top approaches the hat-function PoU. Consequently, the higher order SGFEM turns into the SGFEM. However, the scaled condition number increases since the complete polynomial enrichment is used. To illustrate such an effect, the SCN is presented in Figure 16.

Figure 16 – L-shaped panel: scaled condition number for σ analysis

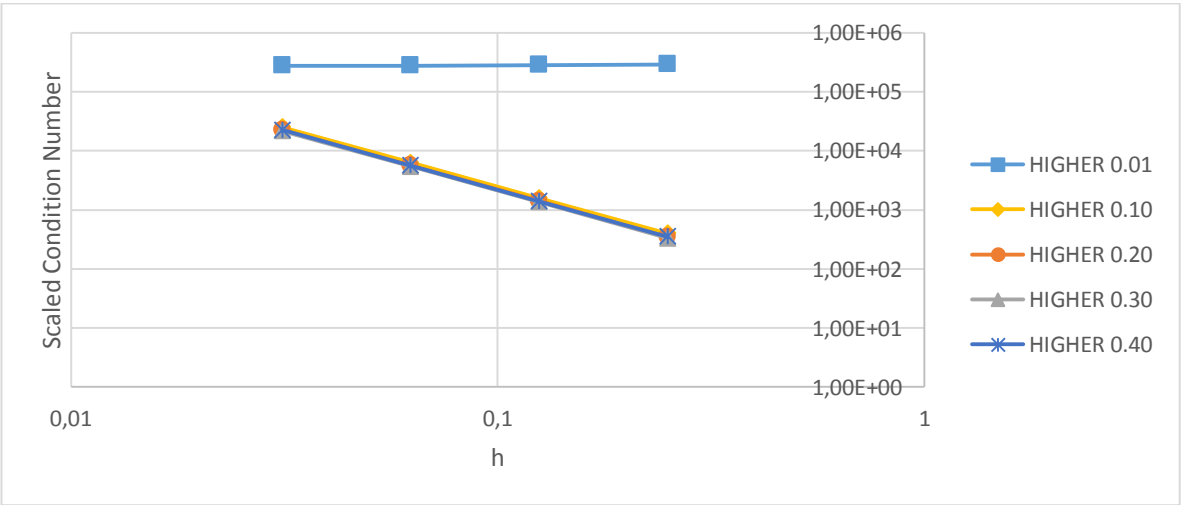

In conclusion, concerning the values of σ adopted, there is practically no difference between the h-convergence curves. However, when considering $\sigma \leq 0.01$, the SCN increases comparatively, already for the coarse mesh, and the solution is therefore less reliable. Since $\sigma = 0.1$ was shown to have the lowest value of relative error, this value will be selected for the next conditions.

7.1.2 Polynomial enrichment

Complete and incomplete polynomials of degree two, both in their shifted readings are considered in this section as the enrichment option.

A comparison between the GFEM, SGFEM and higher order SGFEM methods is presented. The rate of convergence based on the estimate relative errors on displacements, as well as the scaled condition number are the main aspects assessed.

The relative errors computed for the case of incomplete polynomial enrichment are reported in Table 2.

Table 2 – L-shaped panel: relative errors for incomplete polynomial

Mesh	h	FEM	GFEM	SGFEM	Higher Order $\sigma = 0.1$
4x2	0.25	0.1423	0.08988	0.07063	0.078560718
8x4	0.125	0.06743	0.03542	0.032	0.034963031
16x8	0.0625	0.03046	0.01567	0.01483	0.016122405
32x16	0.03125	0.0137	0.00711	0.00682	0.007415862
64x32	0.01563	0.00615	0.00318	0.00306	0.003339863
128x64	0.00781	0.00271	0.00135	0.0013	0.001429723

The log x log graphs depicted in Figure 17 show the h-convergence of the relative errors for the case of incomplete enrichment. It must be pointed out that this is not a regular problem as the reentrant corner of the L-shaped panel induces stress singularity. Even so, it can be observed that comparing GFEM and SGFEM versions to the FEM, the convergence rates are pretty much of the same order.

Figure 17 – L-shaped panel: h-convergence for incomplete polynomial

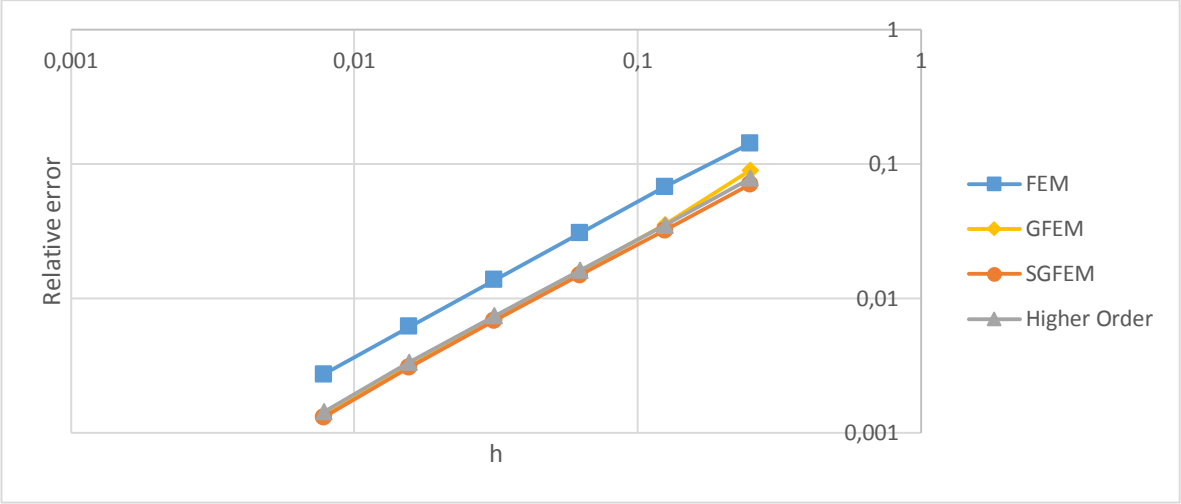

In terms of comparative gains, the relative errors provided by the GFEM or SGFEM are very close in values to the ones obtained through FEM, however demanding a mesh one level coarser. Therefore, analyzing the number of degrees of freedom used for this example, both the GFEM/SGFEM spent less DoF obtaining the same relative error, as shown in Table 3. Of course, this reduction in the DoF implies in a low processing time.

Table 3 – L-shaped panel: degrees of freedom for incomplete polynomial

Mesh	h	FEM	GFEM/SGFEM
4x2	0.25	42	126
8x4	0.125	130	390
16x8	0.0625	450	1350
32x16	0.03125	1666	4998
64x32	0.01563	6402	19206
128x64	0.00781	25090	75270

Another remarkable measure is the scaled condition number. If comparable to the FEM values, SCN indicates stability of the GFEM/SGFEM linear system. Figure 18 shows the SCN for the methods using the incomplete enrichment. It is observed that the values obtained for the GFEM, SGFEM and higher order SGFEM are close to the FEM values. Indeed, the SGFEM versions do not present any advantage over the GFEM, since the incomplete enrichment verifies the linear independence condition already for the GFEM.

Figure 18 – L-shaped panel: scaled condition number for incomplete polynomial

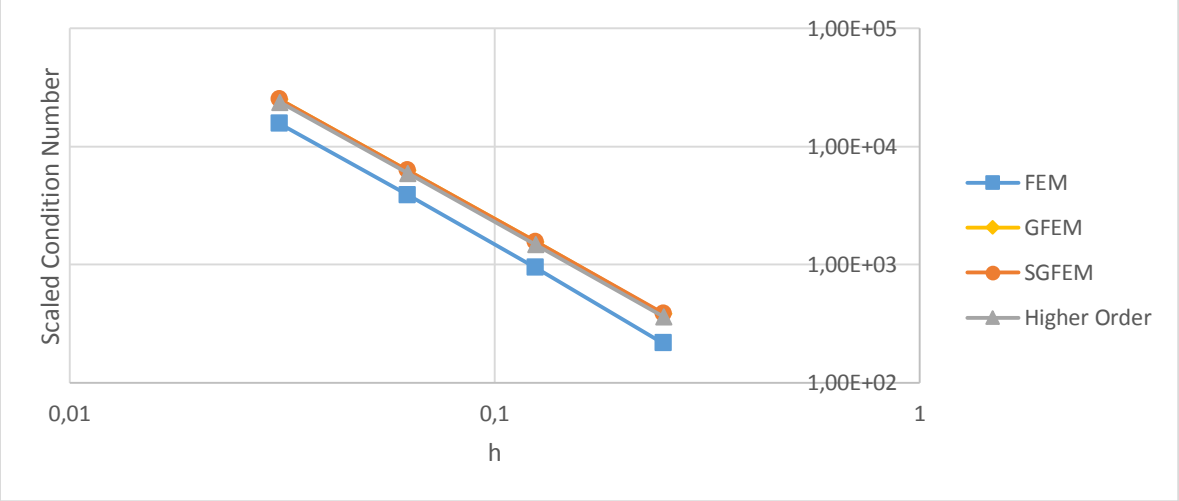

However, as reported in Table 4, when a complete enrichment is considered, the SCN is strongly affected in the SGFEM, which remains comparable to the bad condition level shown by GFEM. This is evidence that the resulting enriched space lacks linear independence property. However, this property is provided to the enrichment space when the flat-top PoU is used and this advantage can be observed by the decrease in the SCN values, comparable to the FEM ones.

Table 4 – L-shaped panel: scaled condition number for complete polynomial

Mesh	h	FEM	GFEM	SGFEM	Higher Order $\sigma = 0.1$
4 x 2	0,25	2.16E+02	3.87556E+16	4.00E+16	4.02E+02
8 x 4	0,125	9.43E+02	1.37449E+17	2.19E+15	1.59E+03
16 x 8	0,0625	3.87E+03	1.69705E+17	8.10E+15	6.34E+03
32 x 16	0,03125	1.56E+04	4.05187E+17	6.59E+17	2.53E+04

Although using the flat-top PoU results in a well-conditioned matrix, as a consequence of its limited capacity of approximation, the relative error is a little higher than that obtained through SGFEM, as shown in Figure 19.

Figure 19– L-shaped panel: h-convergence for complete polynomial

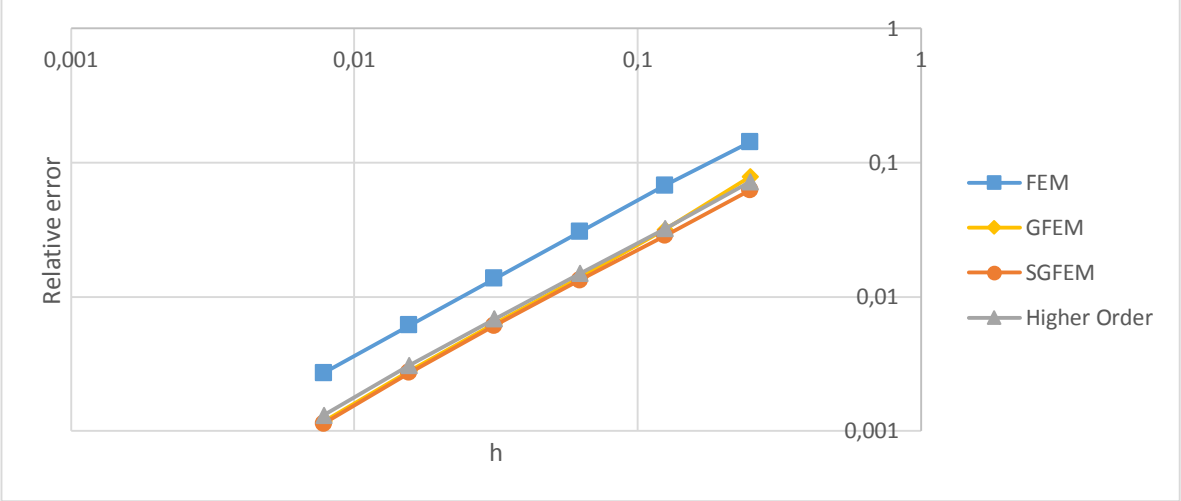

7.1.3 Singular enrichment

The singular enrichment function is applied locally in the neighborhoods of the reentrant corner. The application is made in a three layer scheme, defined as follows:

a) Layer 0 (L0): only the node at the corner is enriched;
b) Layer 1 (L1): all the nodes of the elements containing the corner are enriched;
c) Layer 2 (L2): in addition to layer 1, all the nodes of elements adjacent to it are enriched.

These layers are shown in Figure 20.

Figure 20 – L-shaped panel: layer representation (a) Layer 0, (b) Layer 1 and (c) Layer 2. The red dots highlight the enriched nodes

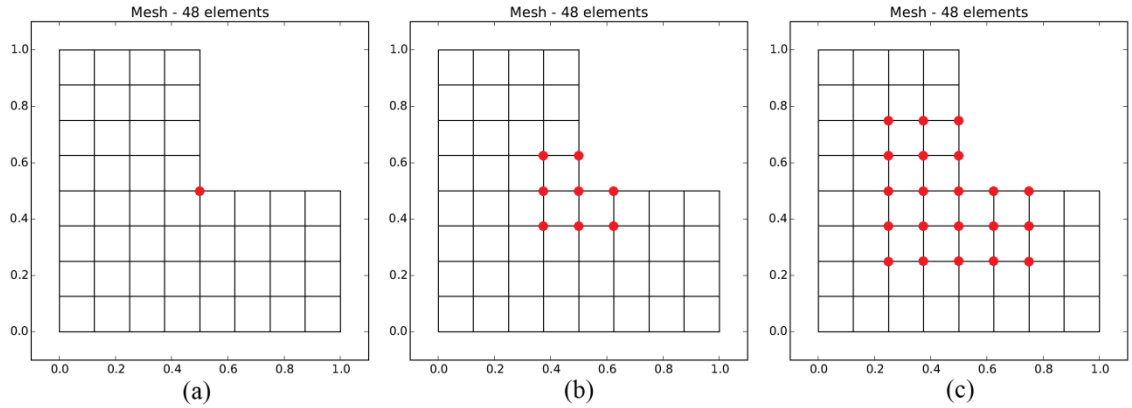

For each layer case, an analysis is made regarding the effect of different values of n_{singular}, related to the number of terms for defining the singular function. Moreover, a comparison between the GFEM and SGFEM is presented. In both cases, the main aspect evaluated is the rate of convergence based on the relative error on displacement.

For the case of the L-shaped panel, the singular enrichment function given in relation (17) is such that Γ_1 and Γ_2 are both Neumann boundaries and $\gamma = 3\pi/2$. Therefore, the resulting expression reads as below:

$$L_{\alpha(k)} = r^{2k/3} \cdot \cos\left(\frac{2k}{3} \cdot \theta\right) \tag{22}$$

The h-convergences for GFEM considering different layers are presented in Figures 21 to 23. For each layer the parameter n_{singular} varies from 1 to 3. It worth mentioning that when considering $n_{\text{singular}} = 3$, for instance, the enrichment vector is $\{1, L_{\alpha(1)}, L_{\alpha(2)}, L_{\alpha(3)}\}$ and not just as $\{1, L_{\alpha(3)}\}$.

Figure 21 – L-shaped panel: h-convergence for singular layer 0 with different values of n_{singular}

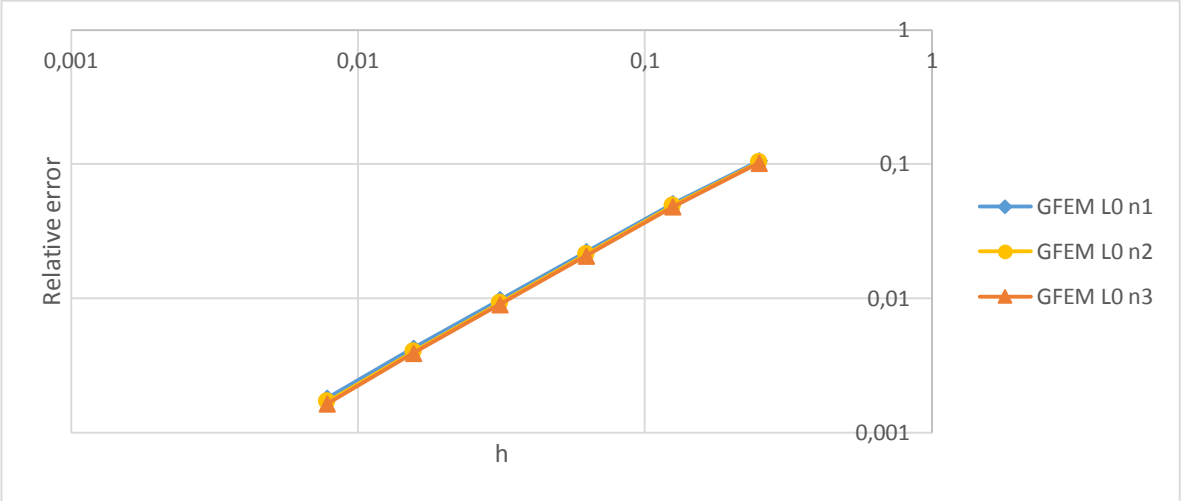

Figure 22 – L-shaped panel: h-convergence for singular layer 1 with different values of n_{singular}

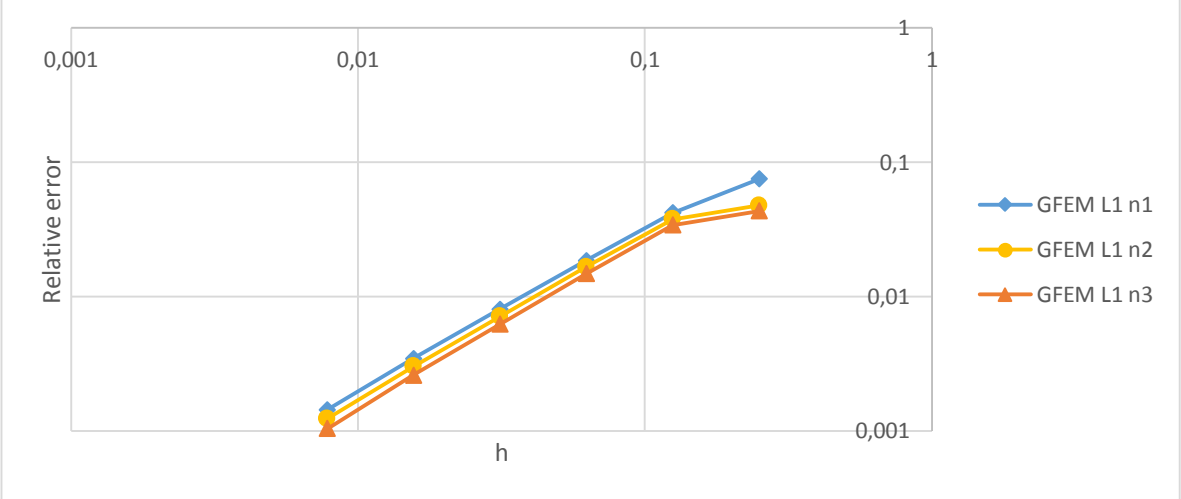

Figure 23 – L-shaped panel: h-convergence for singular layer 2 with different values of n_{singular}

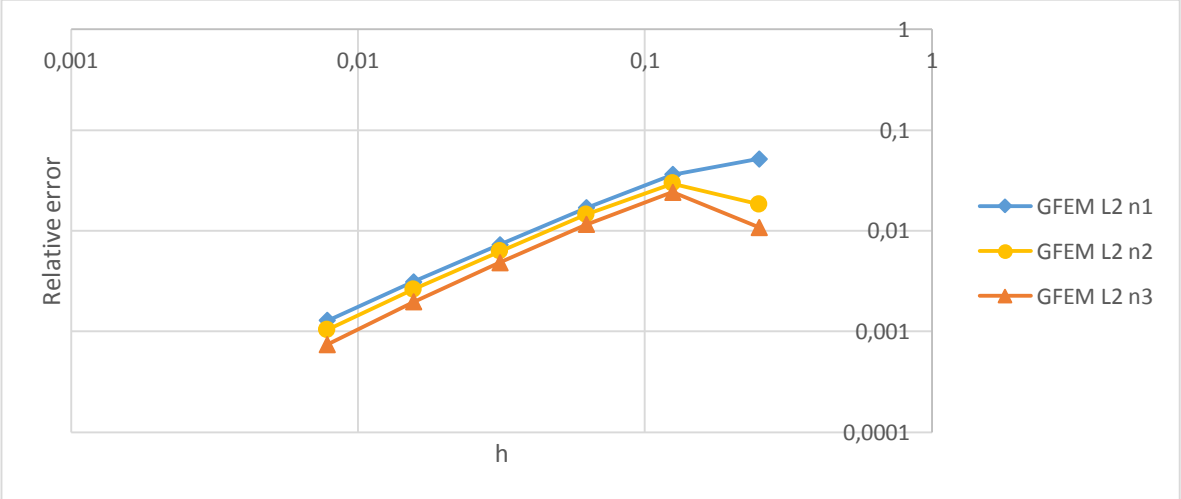

For the different cases presented the rate of convergence is practically the same regardless of the value n_{singular} adopted. Therefore, it is valid to adopt n_{singular} equals to one for the next analysis.

Moreover, the misalignment of the points related to the coarse mesh (4x2) observed in Figures 22 and 23 is supposed to be a consequence of the significant number of enriched nodes included in the layer regarding the total number of nodes in the mesh. Differently from the other meshes, in this mesh, all nodes are enriched when applying layer 2, for instance and no blending elements are presented. Then, the presence of blending elements actually worsens the approximate solution.

Fixing the value of $n_{singular} = 1$ and analyzing the results of h-convergence for GFEM and SGFEM (Figures 24 to 26), the relative error for the SGFEM is slightly reduced and the rate of convergence is slightly greater when compared to the GFEM and FEM rates. This once again can be associated to the blending elements. As in both versions the GFEM and SGFEM blending elements are present, apparently the SGFEM itself is more effective in terms of overcoming the related detrimental effects.

Figure 24 – L-shaped panel: comparison between methods with respect to h-convergence for singular layer 0

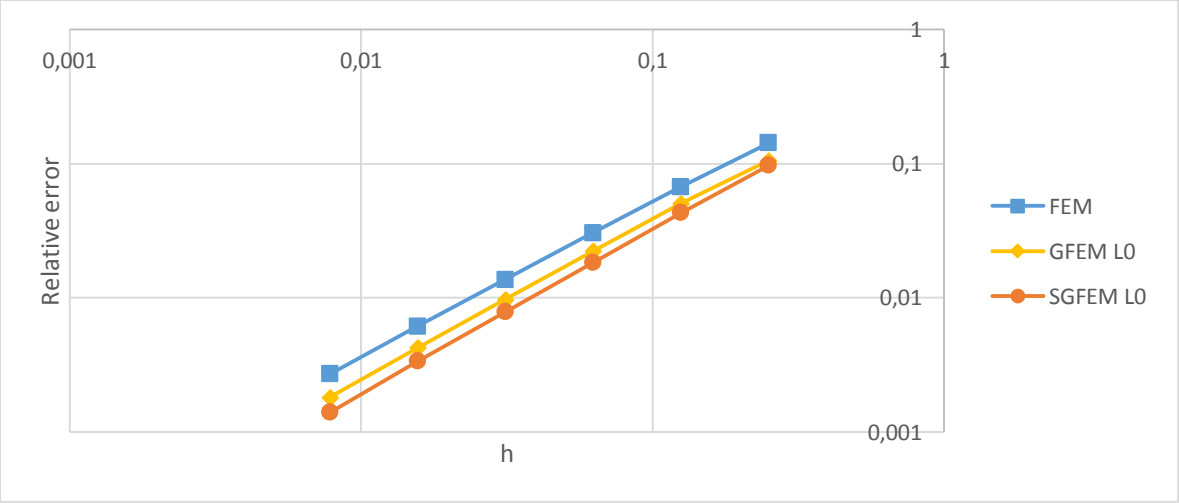

Figure 25 – L-shaped panel: comparison between methods with respect to h-convergence for singular layer 1

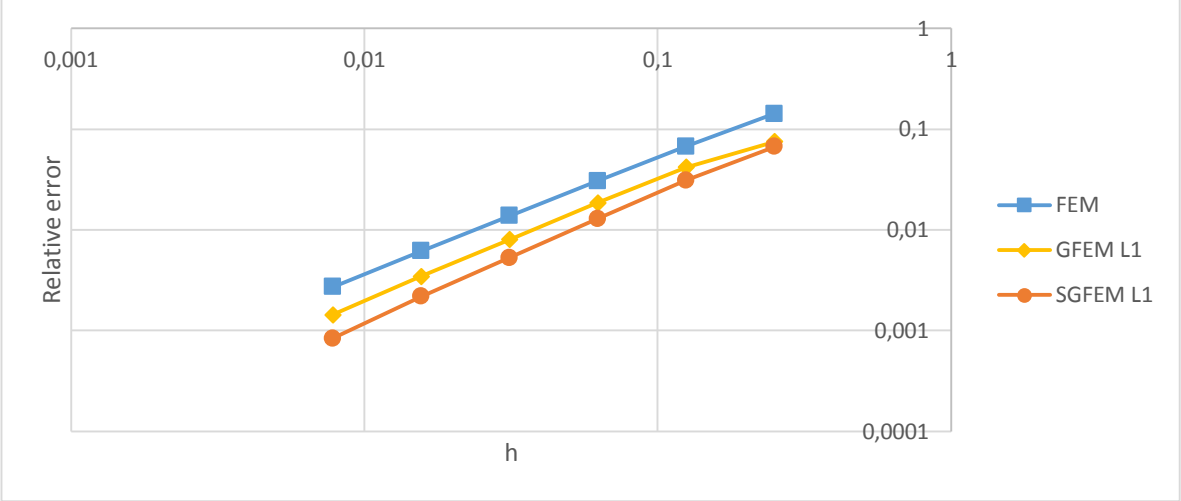

Figure 26 – L-shaped panel: comparison between methods with respect to h-convergence for singular layer 2

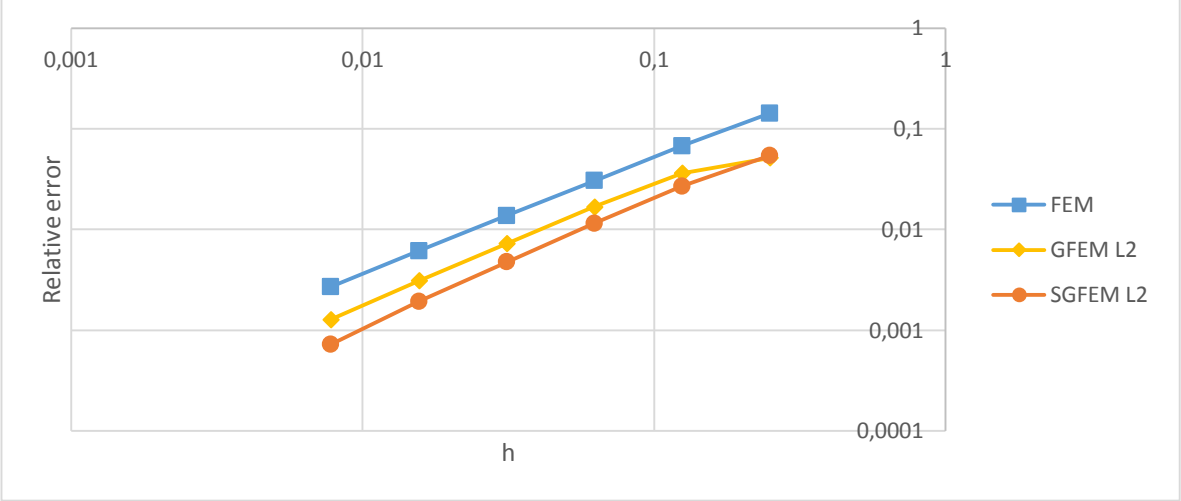

7.1.4 Polynomial and singular enrichment combined

In this section, the possibility provided by the GFEM/SGFEM of augmenting the trial/test spaces with as many functions as necessary for better approximating the solution is explored. The basic aim is to show that the combination of distinct enrichments in specific parts of the panel will contribute to obtain a better approximate solution, therefore dismissing an excessive mesh refinement. Hence, the polynomial enrichment is applied at all nodes of the mesh, since the solution is predominantly smooth in the panel. In addition, the singular enrichment is applied at the part

near the reentrant corner as the response presents significant gradients due to the stress concentration caused by the local geometry.

The analysis of the numerical response will be conducted by controlling the rate of convergence of the relative errors on displacements and also through the SCN.

Figures 27 to 29 show the h-convergence considering the singular enrichment in different layers combined with an incomplete polynomial enrichment of second degree.

Figure 27 – L-shaped panel: comparison for incomplete polynomial and singular layer 0

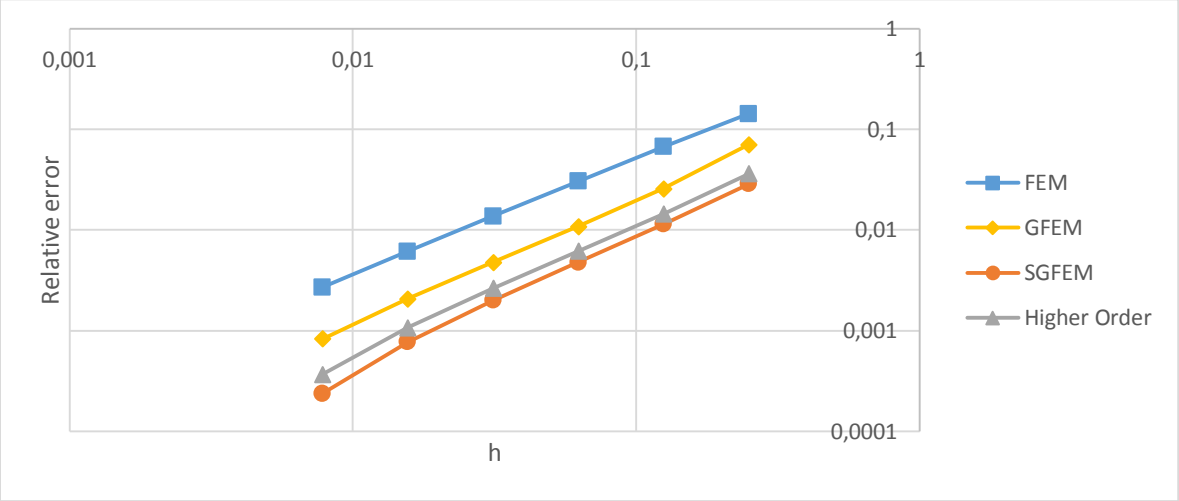

Figure 28 – L-shaped panel: comparison for incomplete polynomial and singular layer 1

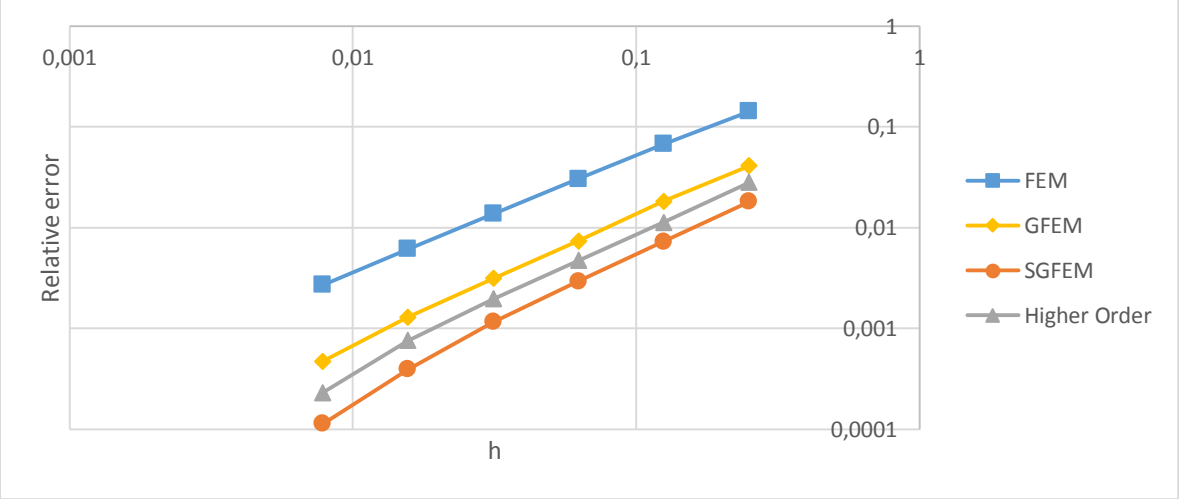

Figure 29 – L-shaped panel: comparison for incomplete polynomial and singular layer 2

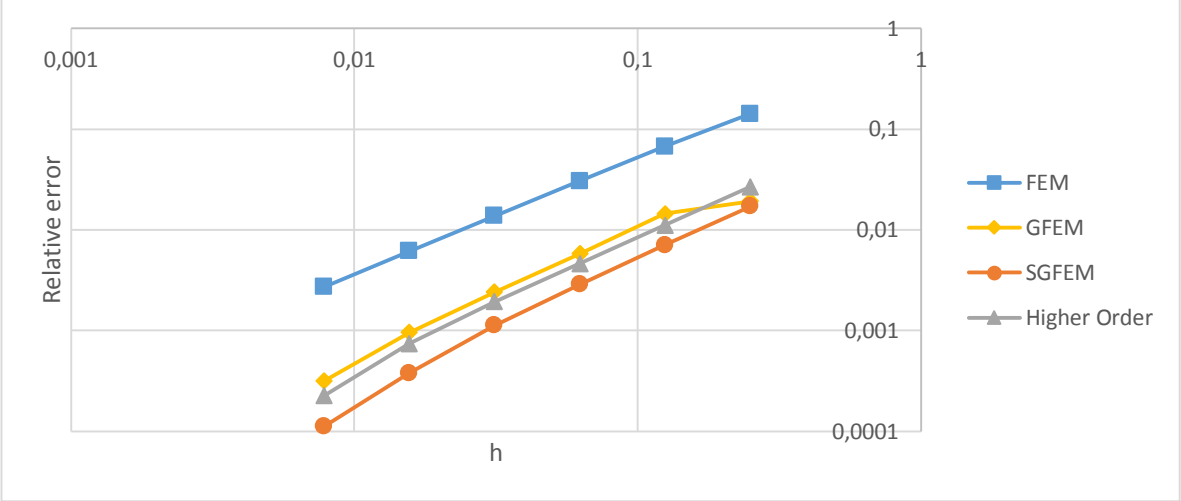

As well as what was observed in the case of single singular enrichment, the h-convergence curve provided by the SGFEM is slightly more inclined, indicating that its response converges more quickly than the FEM. In addition, both enrichments contribute to a clear improvement in the approximate solution with respect to the FEM. Looking at the response shown in Figure 29, considering a same mesh, the SGFEM exhibits a relative error one order of magnitude smaller than the standard FEM.

Moreover, in Figure 29, it is possible to conjecture about the effects of the blending elements. In particular, regarding the first mesh, (4x2), when using the layer 2 option for singular enrichment, all the nodes of the mesh become enriched and consequently, there are no blending elements. As a result of this, the GFEM and SGFEM responses are very close. Nevertheless, in the finer meshes, once blending elements appear, apparently the GFEM response is more affected then SGFEM is, therefore generating an increase in the relative error values.

Regarding the SCN values, when considering layer 0 they are close to ones provided by the FEM for any of the methods, as shown in Figure 30. However, once introducing the singular function to nodes far away from the corner (layers 1 and 2), the SCN number increases significantly, in particular with respect to the coarse mesh, as can be seen in Figures 31 and 32. It can be concluded that probably such enrichment generates shape functions that are almost linearly dependent. However, once again the SGFEM versions prove to be a better option than GFEM.

Figure 30 – L-shaped panel: SCN for incomplete polynomial and singular layer 0

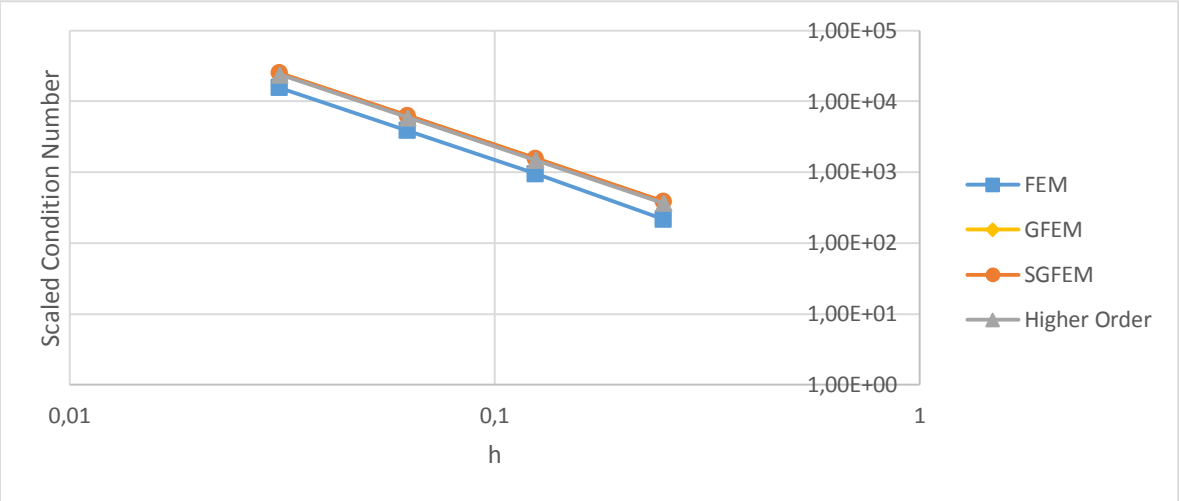

Figure 31 – L-shaped panel: SCN for incomplete polynomial and singular layer 1

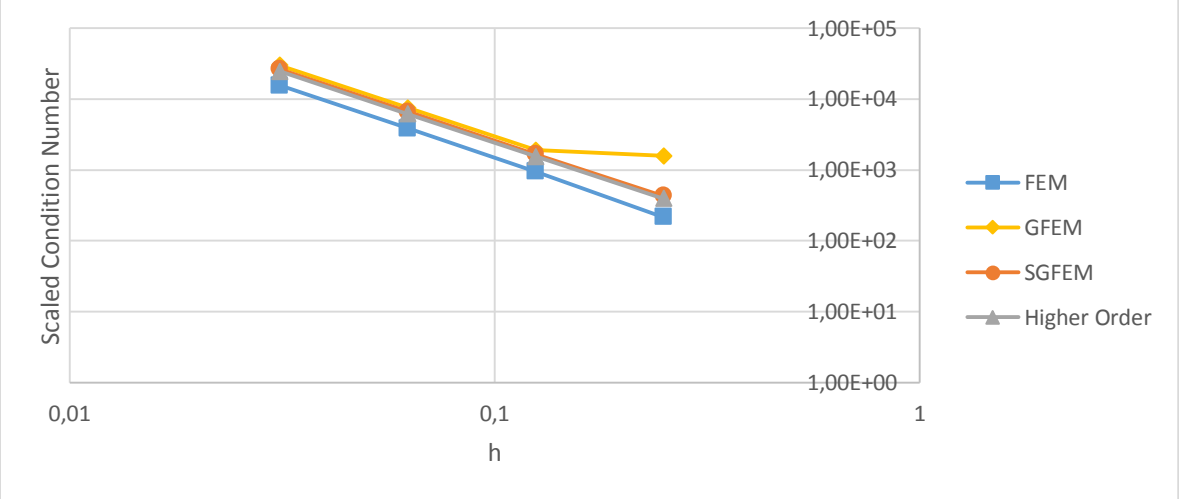

Figure 32 – L-shaped panel: SCN for incomplete polynomial and singular layer 2

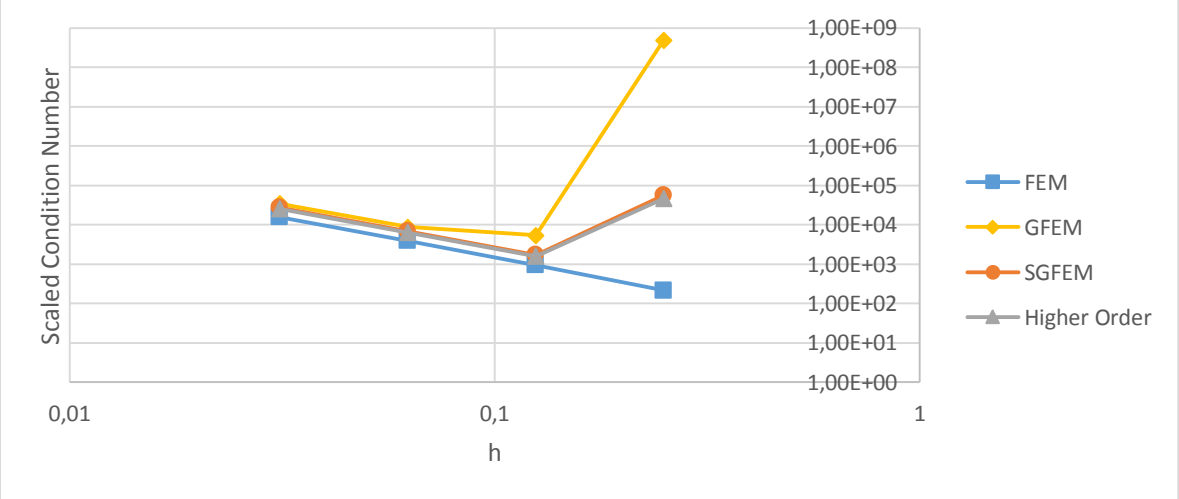

Finally, when considering the complete polynomial enrichment, as expected, the SCN for the GFEM and SGFEM are strongly affected, therefore resulting in a bad conditioned stiffness matrix. Nevertheless, the higher order SGFEM preserves a SCN close to that one obtained for FEM, as reported in Table 5.

Table 5 – L-shaped panel: SCN for complete polynomial and singular layer 2

Mesh	h	FEM	GFEM	SGFEM	Higher Order $\sigma = 0.1$
4 x 2	0.25	2.16E+02	1.8E+16	8.40E+16	1.19E+05
8 x 4	0.125	9.43E+02	1.08E+16	6.52E+15	1.63E+03
16 x 8	0.0625	3.87E+03	4.78E+14	4.29E+15	6.43E+03
32 x 16	0.03125	1.56E+04	5.07E+16	3.27E+15	2.57E+04

Despite the better conditioning for the Higher order, using the flat-top partition of unity results in a worse approximate solution when compared to the SGFEM, as depicted in Figure 33.

Figure 33 – L-shaped panel: h-convergence for complete polynomial and singular layer 2

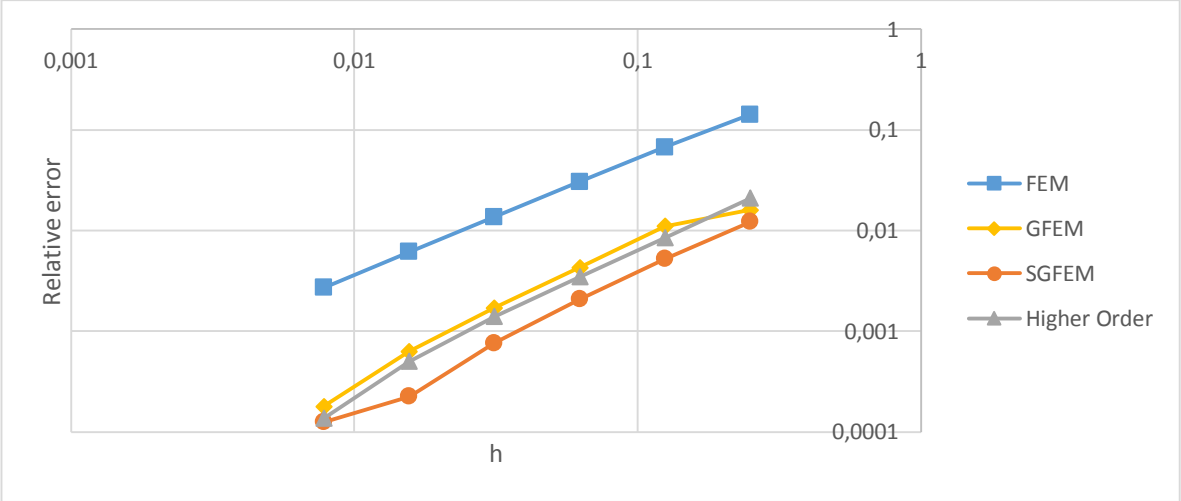

However, the higher order SGFEM benefits from the mesh refinement, as can be seen in Figure 34. Furthermore, the stress concentration due to the singular enrichment is shown in Figure 35.

Figure 34 – L-shaped panel: effect of mesh refinement

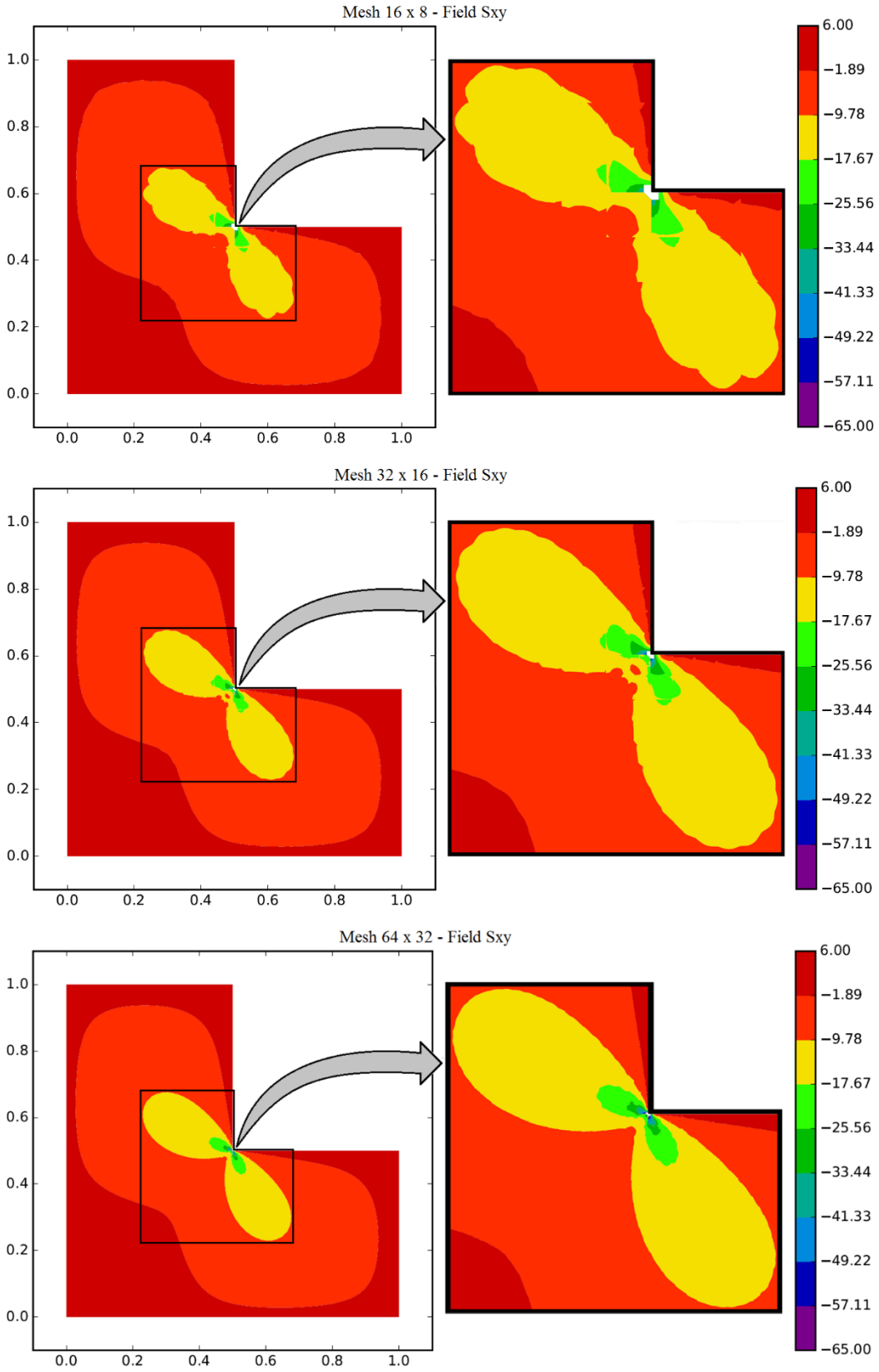

Figure 35 – L-shaped panel: nodal stress Sxy for mesh 64 x 32 using different enrichment

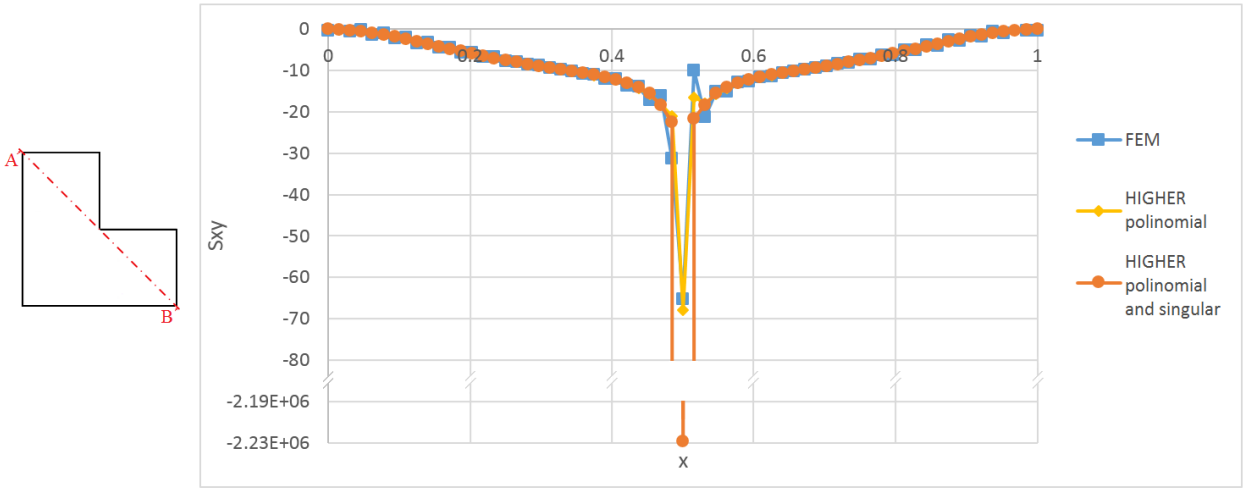

7.2 Panel presenting an edge crack

The selected problem, as well an example of a regular mesh adopted for analysis is depicted in Figure 36.

Figure 36 – Edge cracked panel

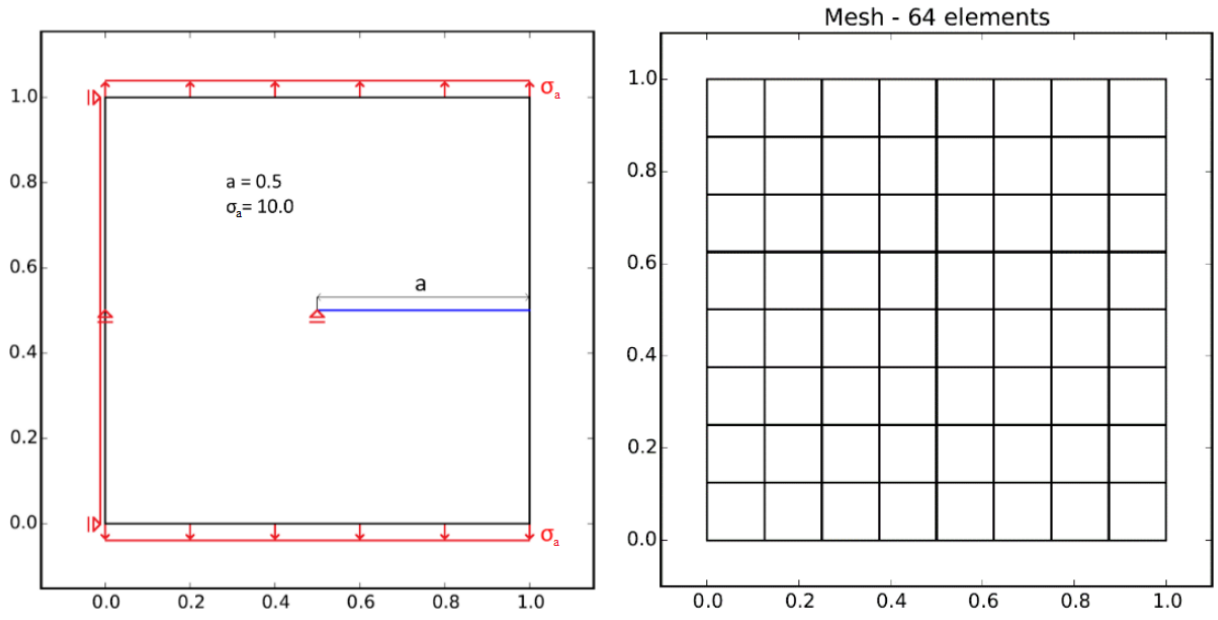

Sliding supports are prescribed at the left Dirichlet vertical boundary and at the crack tip. The Dirichlet boundary conditions are imposed using a penalization technique. Uniform distributed loads are applied at the top and bottom edges. Besides, a gap of 10^{-4} order is considered to represent the crack.

Six structured meshes varying from coarse to fine and composed by bilinear quadrilateral elements are used to analyze the h-convergence, however, for the study of the SCN only the four coarser meshes are considered due to the loss of accuracy for the finer ones. These meshes present the following grid arrangements: 4x4, 8x8, 16x16, 32x32, 64x64 and 128x128, according to the number of elements in the horizontal and vertical directions, respectively.

Analogous to the L-shaped panel, in this example the analysis is made considering four conditions, aiming to focus on the relative differences, advantages and shortcomings, among the GFEM versions.

7.2.1 σ Parameter analysis

The analysis is presented next in terms of the convergence rates of relative errors in displacements for σ equals to 0.01, 0.1, 0.2, 0.3 and 0.4. The enrichment considered is the shifted complete second degree polynomial.

The reference solution u_{ref} used in Relation (21) was computed through FEM using a very refined structured mesh of (2048x2048) elements. The resulting h-convergence curves are presented in Figure 37.

Figure 37 – Edge cracked panel: h-convergence for different values of σ

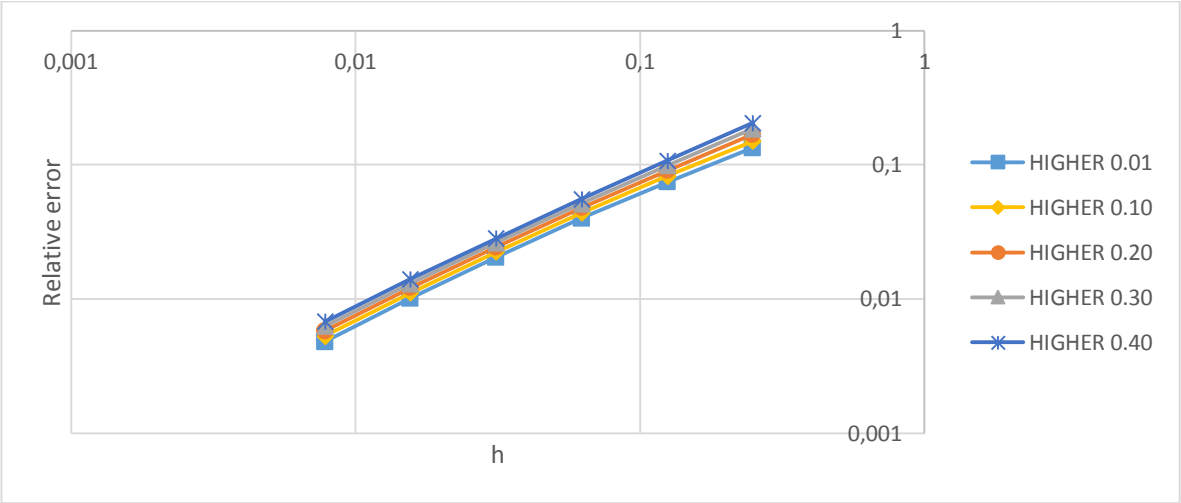

As well as in the L-shape example, the smaller the σ is, the better the approximate solution. However, if σ becomes too small, the partition of unity tends to be pretty much similar to the hat PoU. Then, the scaled condition number increases relatively, already for the coarse mesh, as seen in Figure 38.

Figure 38 – Edge cracked panel: SCN for σ analysis

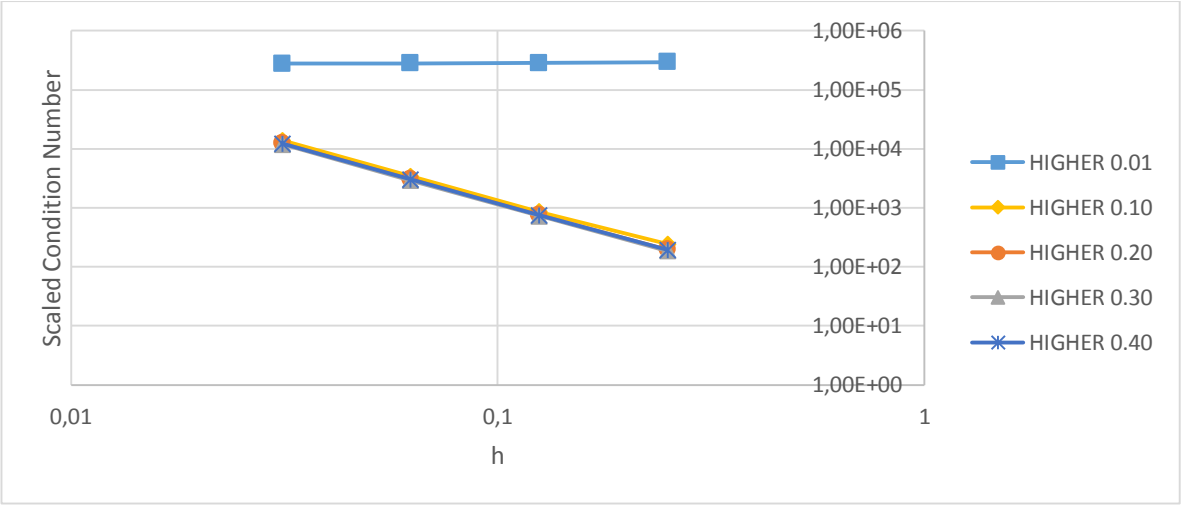

Despite the similarity of the obtained results when comparing the different values of σ in the range from 0.1 to 0.4, a small relative difference can be observed. Therefore, $\sigma = 0.1$ is chosen for the next analysis, since comparatively this value has provided the smallest error and the lowest SCN.

7.2.2 Polynomial enrichment

Shifted complete and incomplete second degree polynomials are considered in this example for the enrichments applied to the whole set of nodes.

A comparison between GFEM, SGFEM and higher order SGFEM is presented. The main aspects appraised are the rate of convergence based on the estimated errors in displacements and the scaled condition number.

The relative errors in displacements were computed using the ℓ_2 norm. For the case of incomplete enrichment, the resulting values are reported in Table 6.

Table 6 – Edge cracked panel: Relative errors for incomplete polynomial enrichment

Mesh	h	FEM	GFEM	SGFEM	Higher Order $\sigma = 0.1$
4x4	0.25	0.26134	0.17022	0.15184	0.166581834
8x8	0.125	0.14344	0.08548	0.08275	0.089600582
16x16	0.0625	0.07421	0.04378	0.04392	0.047327711
32x32	0.03125	0.03741	0.02209	0.02247	0.024203718
64x64	0.01563	0.01853	0.01088	0.01113	0.012011457
128x128	0.00781	0.00898	0.00515	0.0053	0.005740655

The log x log graphs depicted in Figure 39 show the h-convergence of the relative errors. Even if this is not a regular problem, as the crack tip induces heavy stress singularity, it can be observed that the convergence rates are pretty much of the same order comparing the GFEM versions with FEM.

Figure 39 – Edge cracked panel: relative error values for incomplete polynomial and mesh refinement

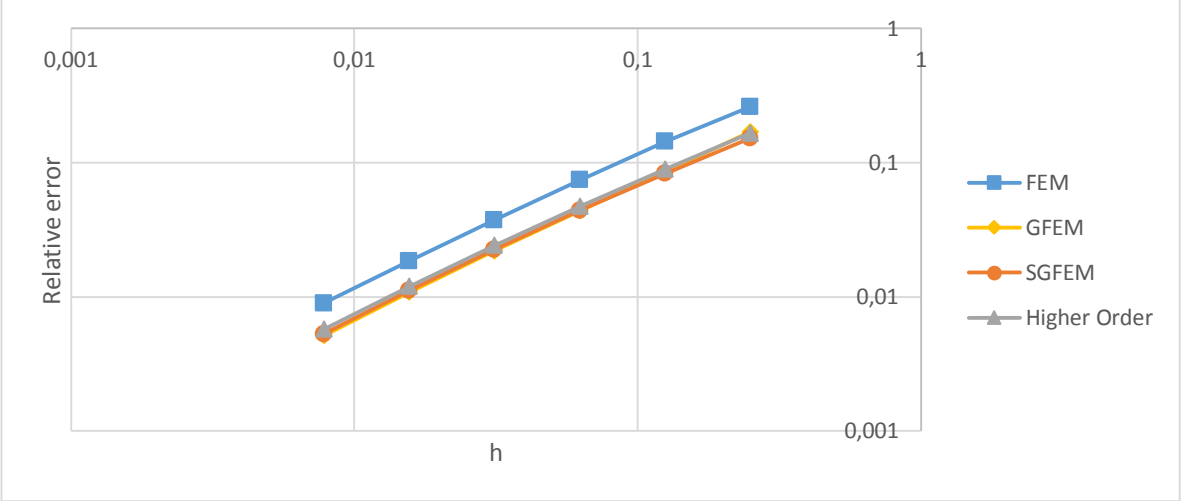

In Figure 40, the scaled condition number is compared still considering the incomplete enrichment case. It can be seen that the values obtained with GFEM versions are of the same order as the values provided by FEM analysis. Once the shape functions resulting from the incomplete enrichment space verify the linear independence condition, in fact the flat-top option does not have any advantage over the SGFEM.

Figure 40 – Edge cracked panel: scaled condition number for incomplete polynomial and mesh refinement

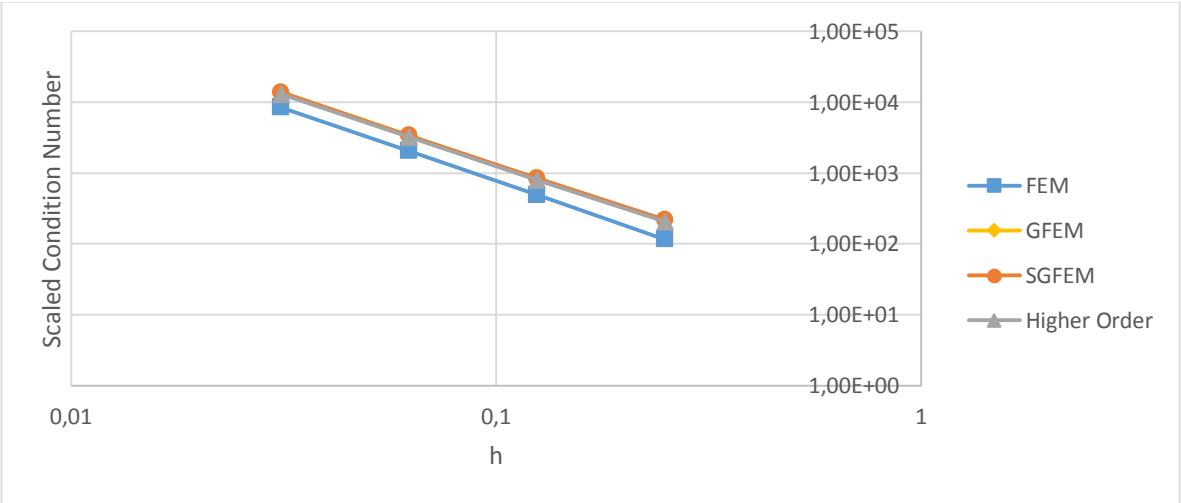

However, when considering complete second degree polynomial enrichment, the SCN for SGFEM is strongly affected, becoming comparable to the bad condition level shown by GFEM, as reported in Table 7. This is a consequence of the linear dependence among the shape functions introduced by the crossed term of the enrichment functions vector. However, linear independence is preserved

when using flat-Top PoU for constructing the enrichment space. This advantage is clear when observing the low SCN values, which are comparable in order to the values obtained by the FEM.

Table 7 – Edge cracked panel: scaled condition number for complete polynomial

Mesh	h	FEM	GFEM	SGFEM	Higher Order $\sigma = 0.1$
4 x 4	0,25	1.16E+02	1.02282E+16	3.07E+17	2.44E+02
8 x 8	0,125	4.89E+02	2.89938E+15	1.75E+16	8.58E+02
16 x 16	0,0625	2.05E+03	1.13806E+16	2.62E+14	3.43E+03
32 x 32	0,03125	8.42E+03	1.05935E+17	2.76E+14	1.38E+04

Once more, using the flat-top PoU results in a limited capacity of approximation and the relative error is higher than that obtained for the SGFEM, as depicted in Figure 41.

Figure 41– Edge cracked panel: relative error values for complete polynomial and mesh refinement

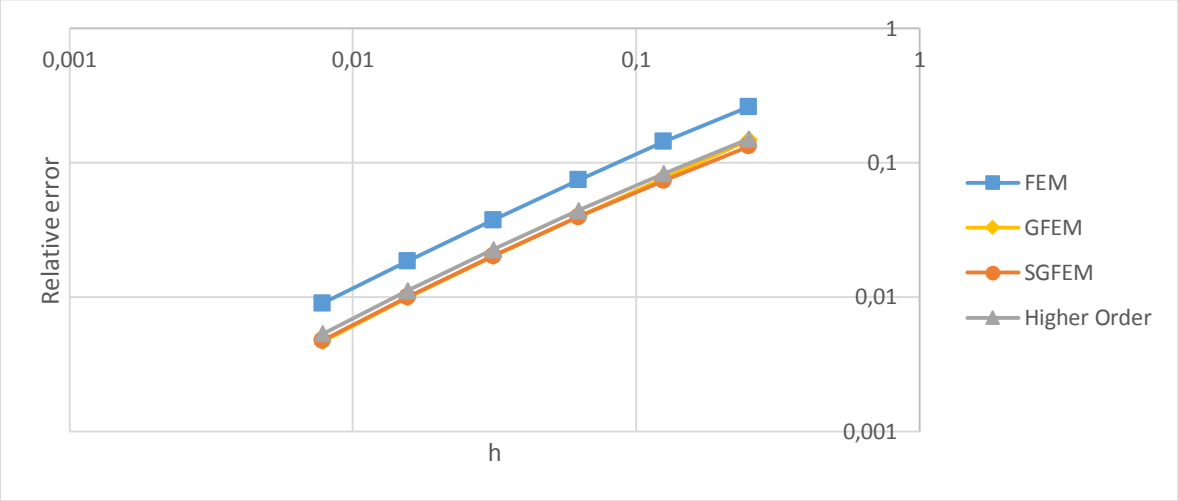

7.2.3 Singular enrichment

Analogous to the L-shaped panel example, the enrichment using the singular function is now applied locally around the crack tip according to a three-layer scheme, as shown in Figure 42.

Figure 42 – Edge cracked panel: (a) Layer 0, (b) Layer 1 and (c) Layer 2. The red dots are the enriched nodes

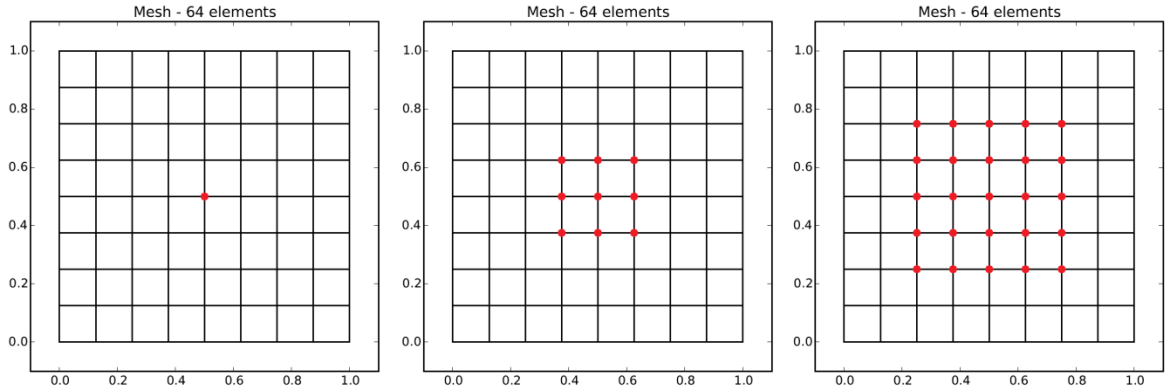

First of all, for each layer case a comparison between different values of n_{singular} is made using only the GFEM. Then, after identifying the more convenient value of n_{singular}, a comparison between the GFEM and SGFEM is presented. In both cases, the comparison is conducted by using the rate of convergence of the relative error.

The singular function parameters for Relation (17) adopted in this example are such that Γ_1 and Γ_2 are both Neumann boundaries and $\gamma = 2\pi$. The resultant enrichment function is:

$$L_{k(\alpha)} = r^{k/2} \cdot \cos\left(k/2 \cdot \theta\right) \tag{23}$$

The h-convergence curves for different layers are presented in the log x log graphs of Figures 43 to 45. For each layer the value of n_{singular} varies from 1 to 3.

Figure 43 – Edge cracked panel: h-convergence for singular layer 0 with $n_{singular}$ varying from 1 to 3

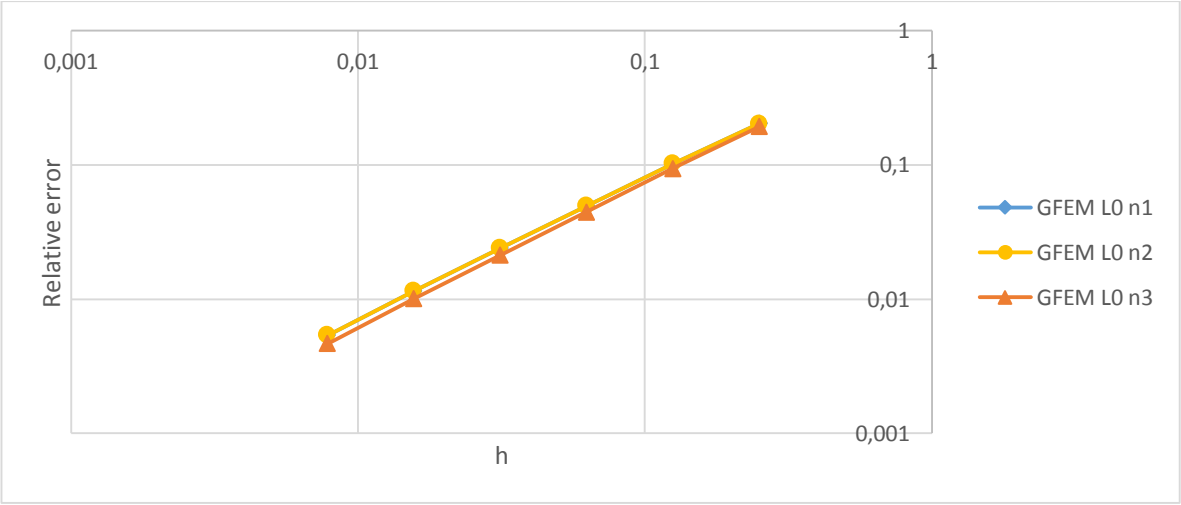

Figure 44 – Edge cracked panel: h-convergence for singular layer 1 with $n_{singular}$ varying from 1 to 3

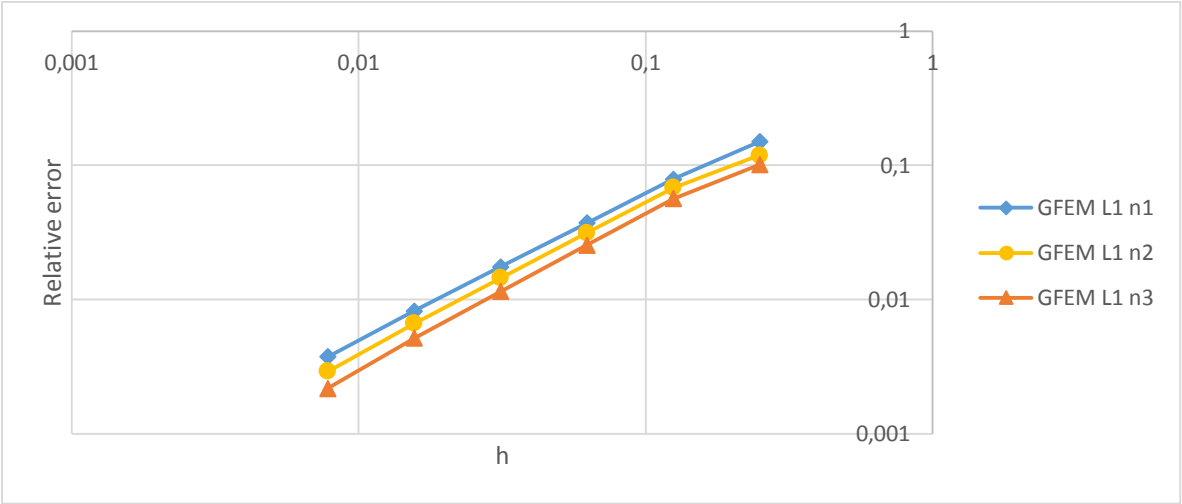

Figure 45 – Edge cracked panel: h-convergence for singular layer 2 with $n_{singular}$ varying from 1 to 3

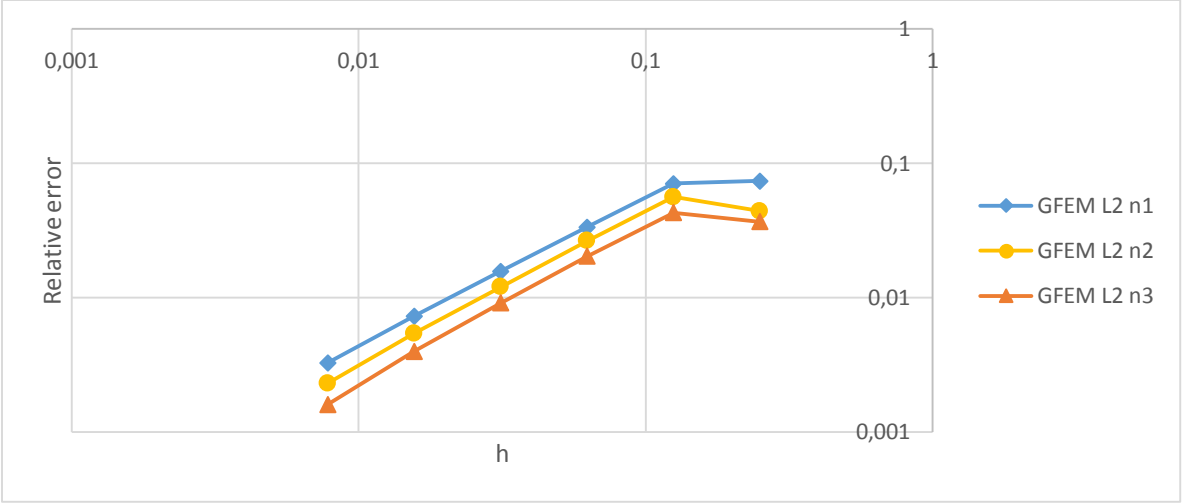

The rate of convergence slightly improves when increasing the value of n_{singular} adopted. Therefore, looking for a good compromise between precision and reduced computational costs, it is valid to adopt n_{singular} equals to one for the next analysis.

Once again, the misalignment of the points related to the coarse mesh (4x4) observed in Figure 45 in particular is supposed to be consequent from the significant number of enriched nodes included in the layer regarding the total number of nodes in the mesh. Differently from the other meshes, in this mesh all nodes are enriched when applying layer 2, for instance and no blending elements are presented. However, when passing to the next mesh, the relative error increases as blending elements arise. Moreover, it is important to note that the singular function is good to approximate

only the neighborhood of the crack tip. Therefore, no significant gain of approximation can be noted in the region far away from crack tip.

In Figures 46 to 48, the h-convergence curves for GFEM and SGFEM are presented using different layers and setting $n_{singular}$ = 1. It is clear that the SGFEM is able to overcome the shortcoming caused by the blending elements.

Figure 46 – Edge cracked panel: comparison between methods with respect to h-convergence for singular layer 0

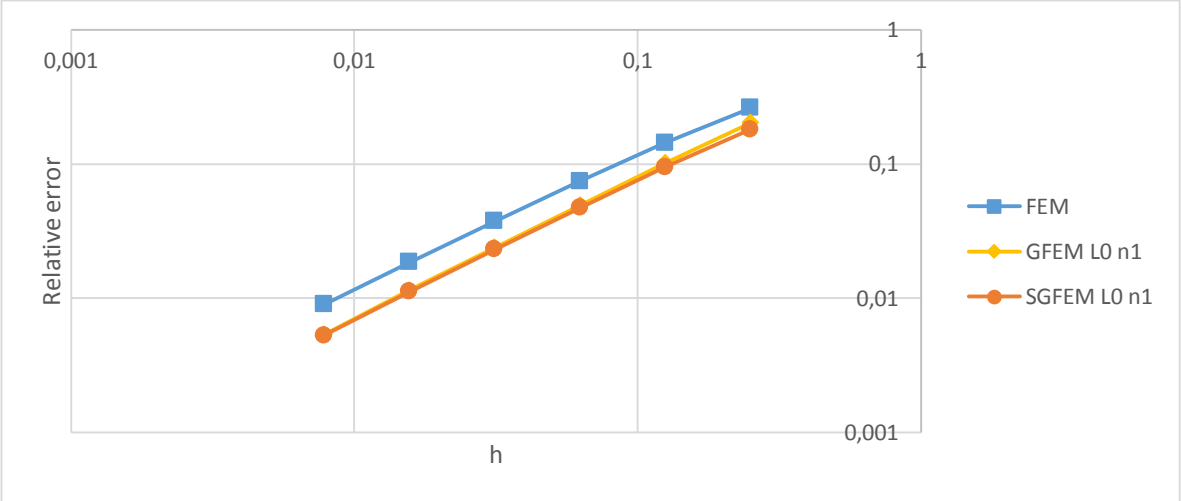

Figure 47 – Edge cracked panel: comparison between methods with respect to h-convergence for singular layer 1

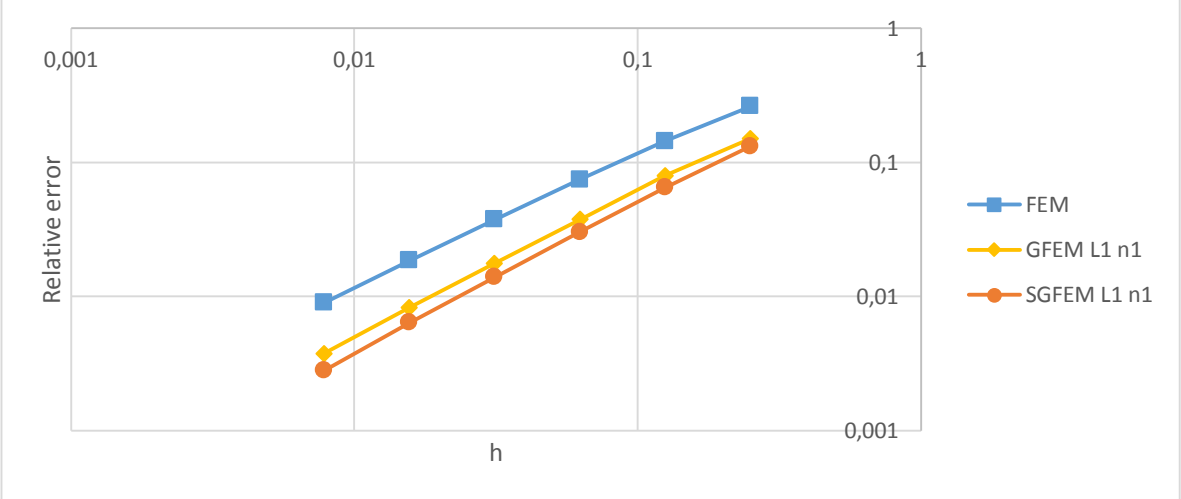

Figure 48 – Edge cracked panel: comparison between methods with respect to h-convergence for singular layer 2

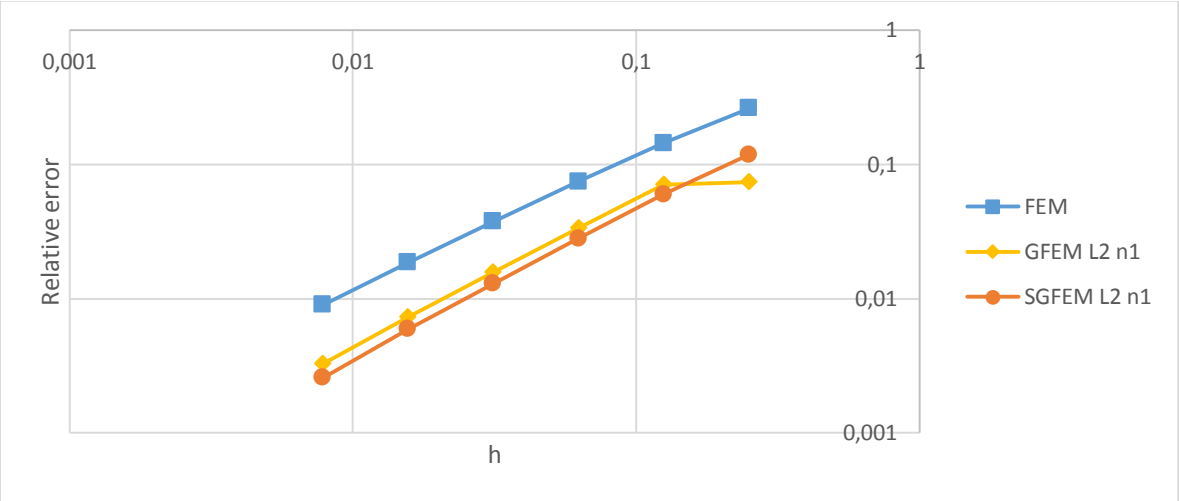

7.2.4 Polynomial and singular enrichment combined

Here both polynomial and singular enrichments are combined. The shifted polynomial is applied to the whole set of nodes, while the singular function is set locally in layers, as in the previous condition.

The analysis is performed with respect to the rate of convergence based on the relative error and the SCN. Figures 49 to 51 show the h-convergence curves resulting from the combination of the singular enrichment in different layers and incomplete polynomial.

Figure 49 – Edge cracked panel: h-convergence curves for incomplete polynomial and singular layer 0

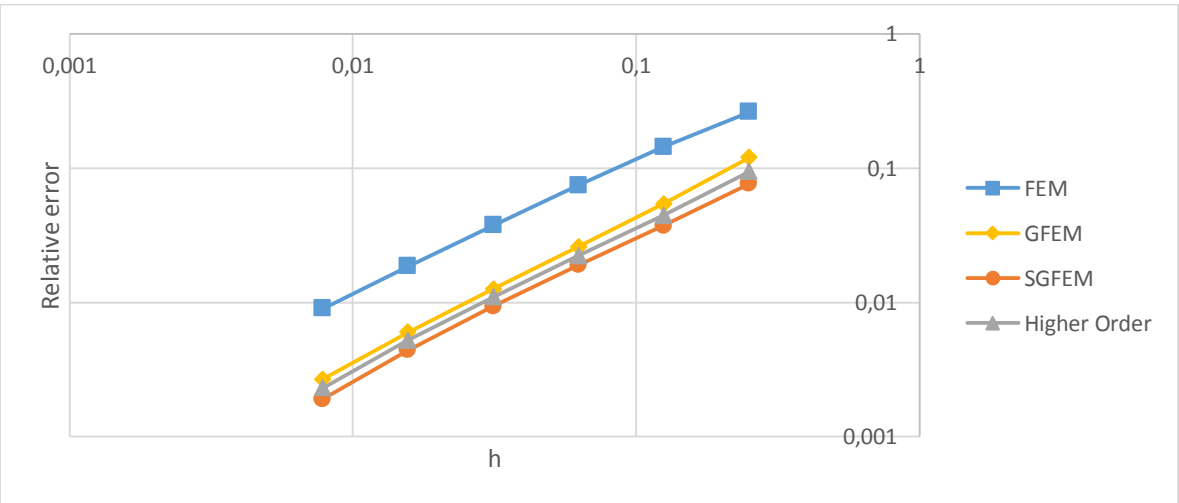

Figure 50 – Edge cracked panel: h-convergence curves for incomplete polynomial and singular layer 1

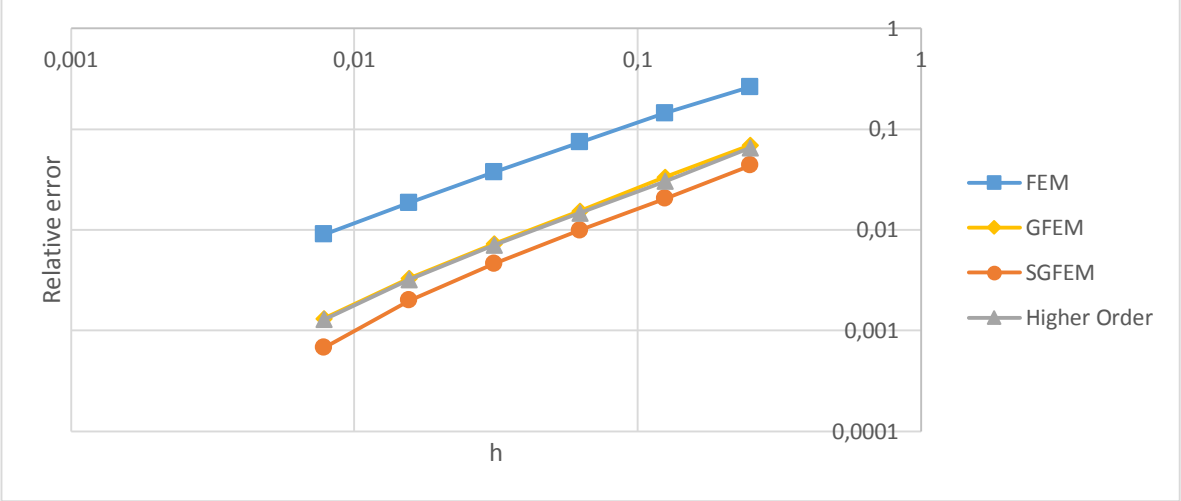

Figure 51 – Edge cracked panel: h-convergence curves for incomplete polynomial and singular layer 2

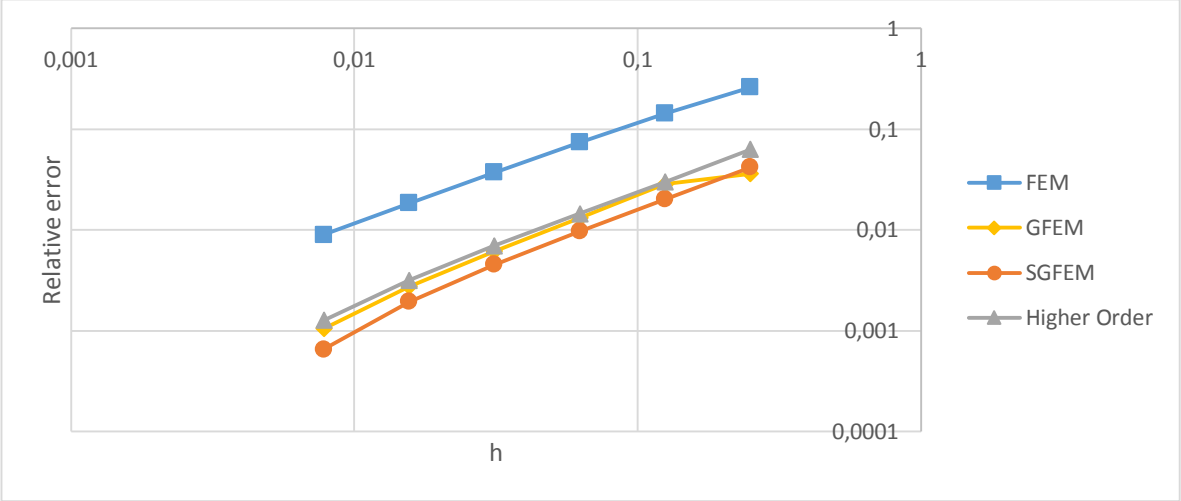

As can be seen in particular in Figure 51 for the GFEM results, the singular enrichment used in a coarse mesh has produced a kind of misalignment of the curve. However, such an effect is not observed in both SGFEM versions. Therefore, apparently these versions are less sensitive to the presence of blending elements.

Although the h-convergence rate for the GFEM versions are similar to the FEM, using these versions are still a good choice due to the fact that the solution can be approximated at an equivalent error level without needing excessive mesh refinement. In fact, as can be seen in the figures above, by already using coarse meshes, the GFEM versions provide solutions similar to the one obtained through FEM using a finer mesh.

Regarding the SCN, while considering singular enrichment restricted to the layer 0 scheme, the results for the GFEM versions are close to numbers provided by the FEM, as shown in Figure 52. However, when the singular function enrichment includes nodes around the corner, the SCN is badly affected, especially for coarse meshes, as can be observed in Figures 53 and 54. Probably, the enrichment combination generates shape functions that are almost linearly dependent on those cases. Even so, the higher order SGFEM seems to be a safer option and the relative small disturbances in SCN values should not be taken into account as the main purpose of using the singular function is to capture the stress concentration that occurs in a small neighborhood of the crack tip.

Figure 52 – Edge cracked panel: SCN for incomplete polynomial and singular layer 0

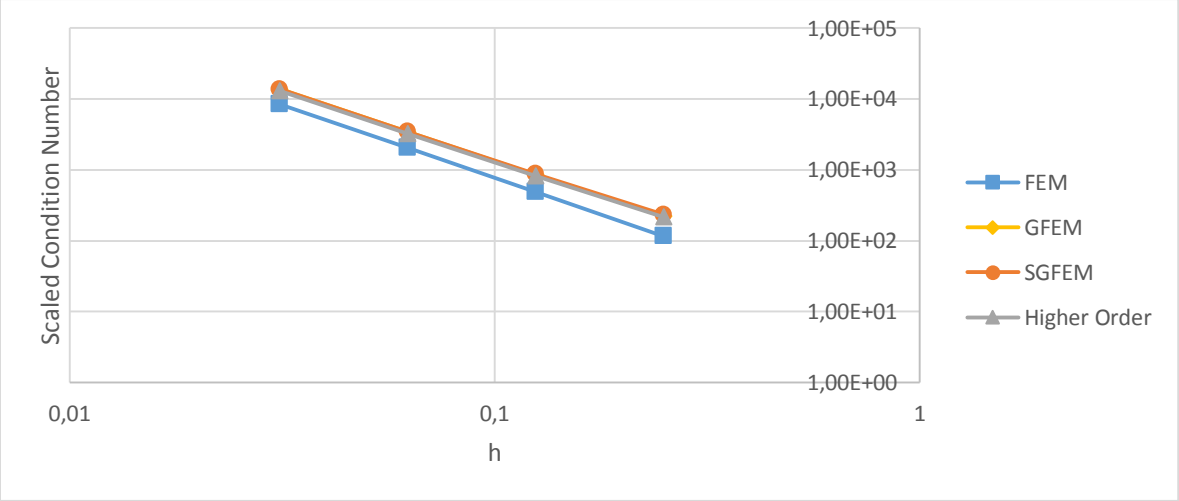

Figure 53 – Edge cracked panel: SCN for incomplete polynomial and singular layer 1

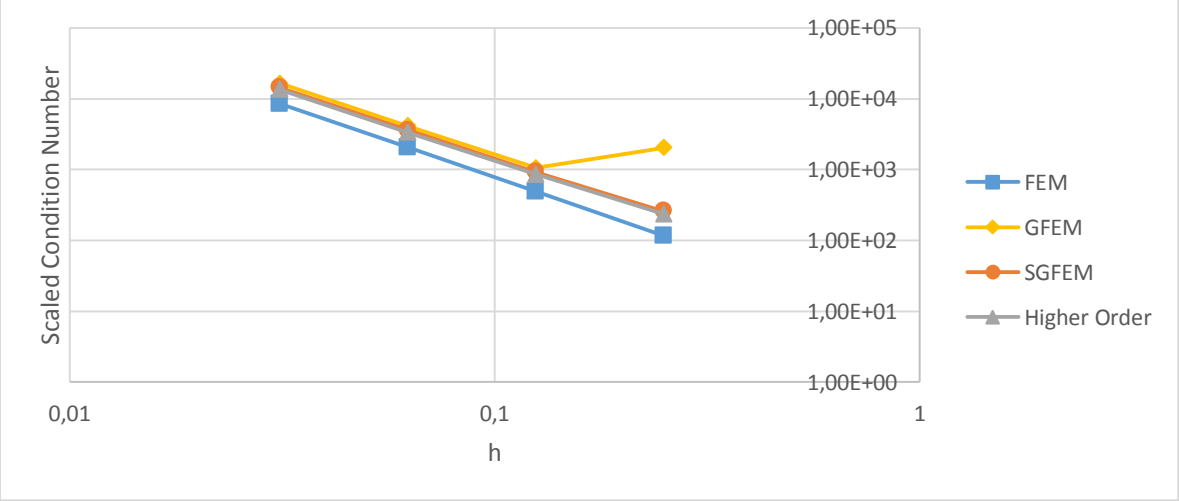

Figure 54 – Edge cracked panel: SCN for incomplete polynomial and singular layer 2

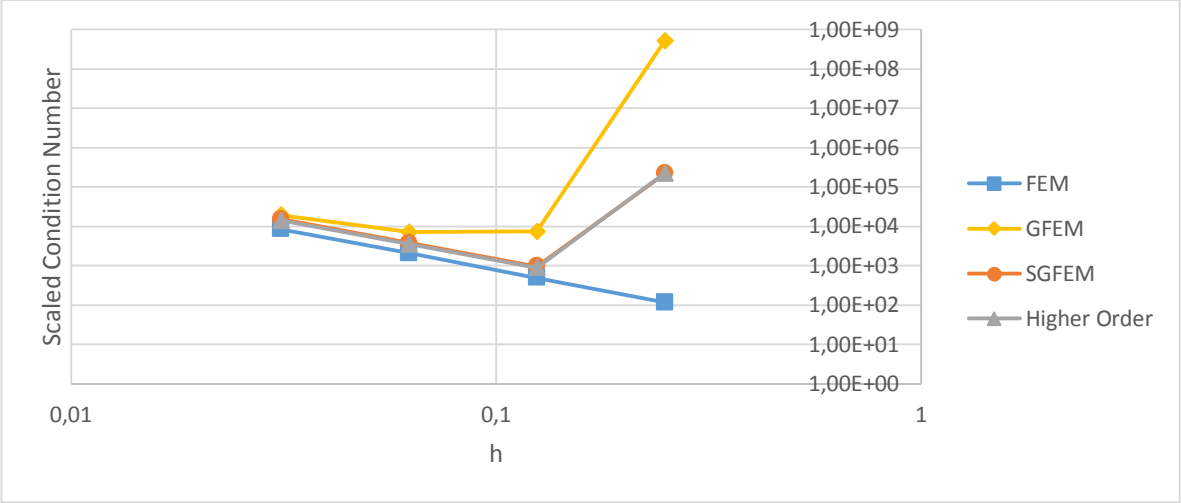

Once again, when considering the complete polynomial, the SCN values for the GFEM and SGFEM are significantly affected. However, the higher order SGFEM keeps a low SCN, with a still acceptable exception for the coarser mesh, as shown in Table 8.

Table 8 – Edge crack panel: SCN for complete polynomial and singular layer 2

Mesh	h	FEM	GFEM	SGFEM	Higher Order $\sigma = 0.1$
4 x 4	0.25	1.16E+02	6.3922E+15	6.07E+15	4.27E+05
8 x 8	0.125	4.89E+02	1.51867E+17	1.26E+18	9.25E+02
16 x 16	0.0625	2.05E+03	1.6821E+16	1.12E+15	3.60E+03
32 x 32	0.03125	8.42E+03	2.4264E+15	5.30E+14	1.44E+04

In fact, despite the relative higher SCN for the coarser mesh when using the higher order SGFEM, this result is still acceptable as it does not point to an ill-conditioned stiffness matrix. Nevertheless, in spite of using the flat-top PoU lead to a well-conditioned system, the relative error obtained is comparatively higher than the error of the SGFEM, as shown in Figure 55.

Figure 55 – Edge cracked panel: h-convergence for complete polynomial and singular layer 2

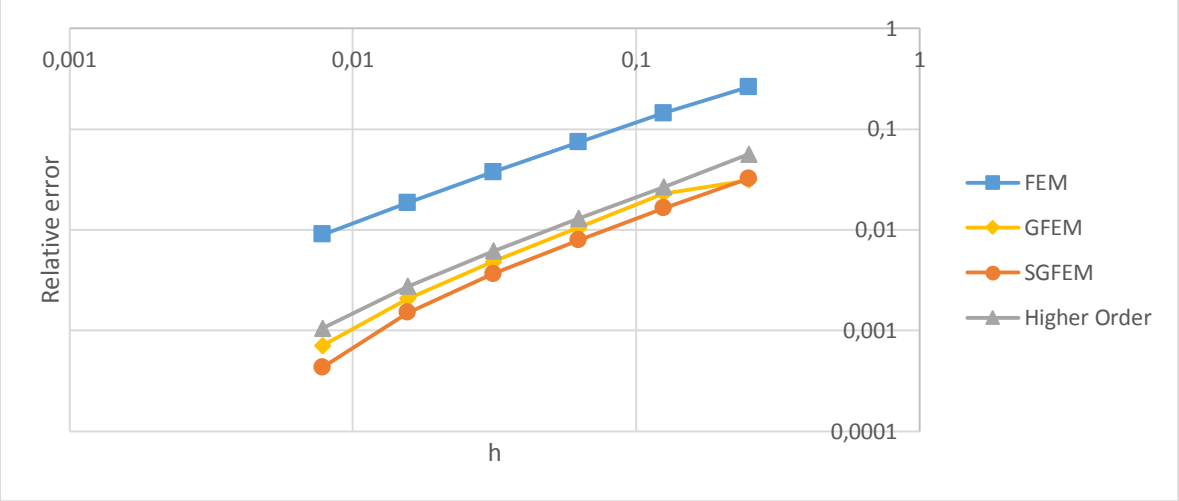

Nevertheless, the SGFEM using flat-Top PoU benefits from the mesh refinement, as shown in Figure 56. Furthermore, the stress concentration due to the singular enrichment is presented in Figure 57.

Figure 56 – Edge cracked panel: effect of mesh refinement

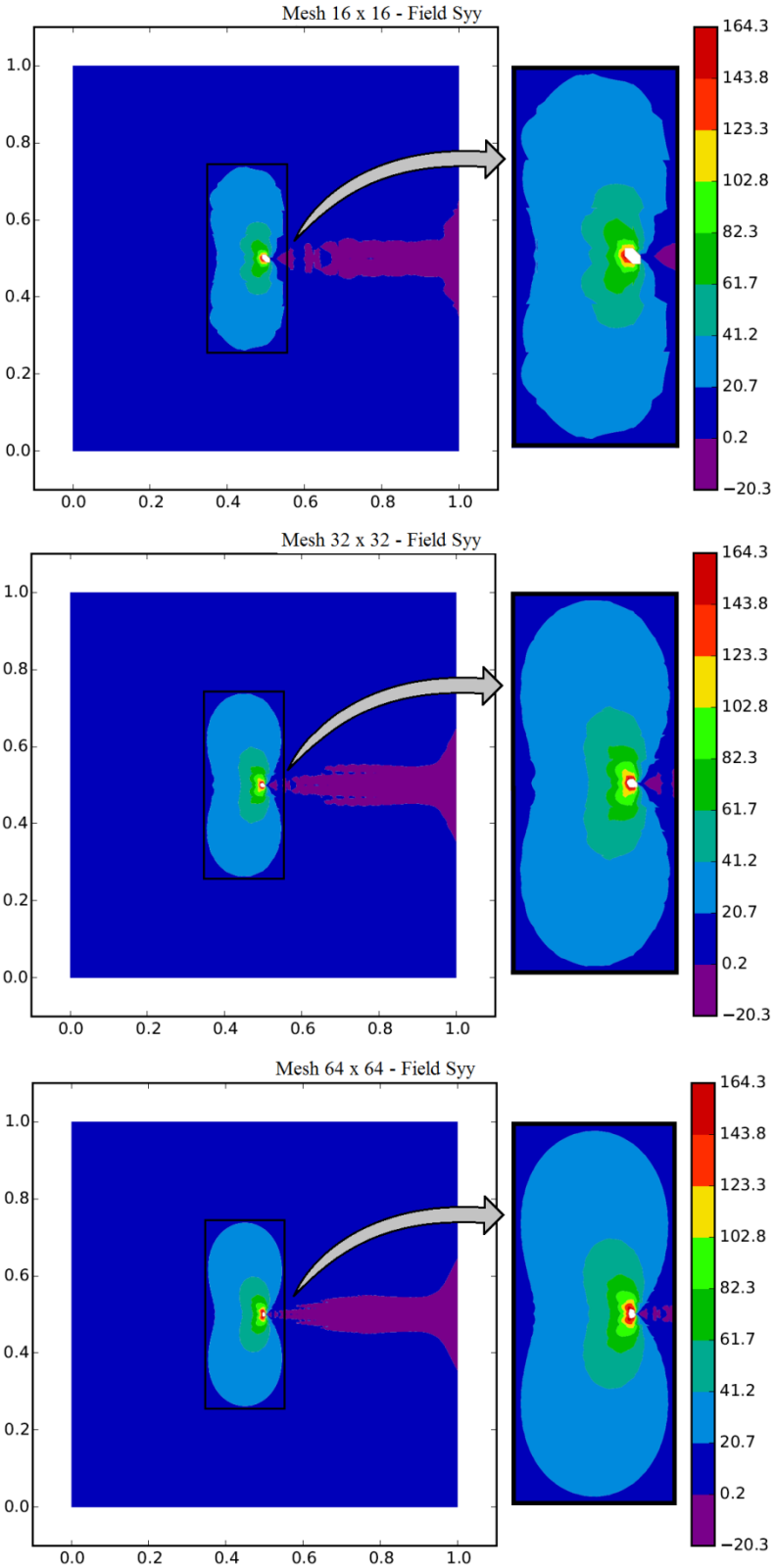

Figure 57 – Edge cracked panel: nodal stress Syy for mesh 64 x 64 for different enrichments

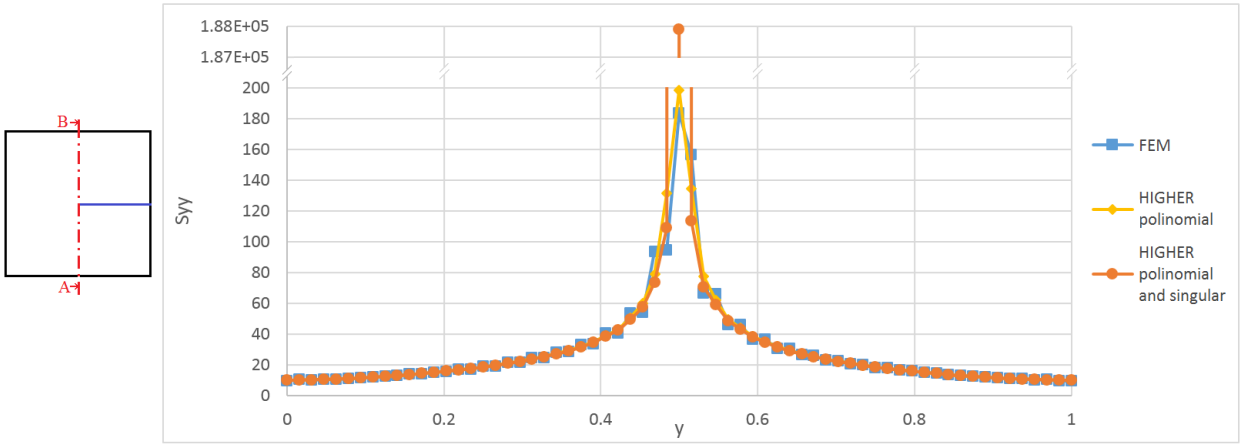

7.3 Panel with multiple corners, polygonal voids and edge cracks

This example aims to show that even if a more complex structure is simulated, the methods hereby considered are still accurate. This example is similar to the test problem originally proposed in Strouboulis, Copps and Babuška (2001). The irregular polygonal geometry is shown in Figure 58a.

Figure 58 – Irregular polygonal panel

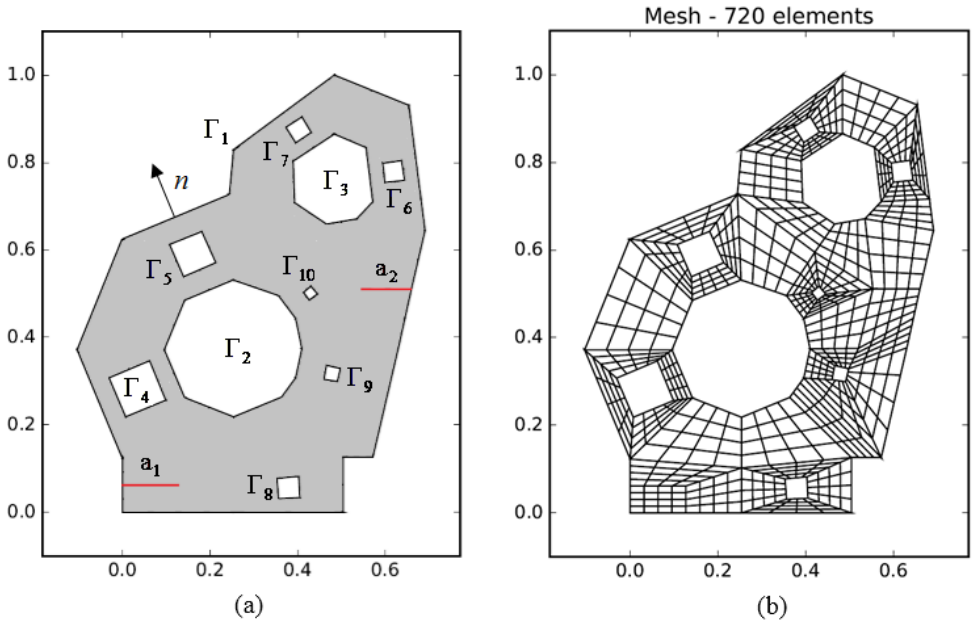

The crack lengths highlighted in red in the figure above are: $a_1 = 0.127$ and $a_2 = 0.107$.

The strong form of the mathematical problem for the linear elasticity, without considering body forces and the respective boundary conditions are defined as follows:

$$div(T) = 0 \text{ on } \Omega$$
$$Tn = q = \nabla(2x - y) \text{ on } \Gamma_1$$
$$u = 0 \text{ on } \Gamma_2$$
$$q = 0 \text{ on } \Gamma_3, \Gamma_4, ..., \Gamma_{10}$$

where T is the stress tensor.

Taking as a reference the preliminary subdivision of the panel domain in subareas, four structured meshes varying from coarse to fine were conceived to analyze the h-convergence rate, each one consisting of bilinear quadrilateral elements. Although, when considering the SCN only the three coarser meshes were considered due to the loss of accuracy for the finer one.

For a better understanding, Figure 59 depicts the areas defined from the preliminary subdivision of the panel domain. The meshes were then successively constructed by dividing the edges of the subareas into 2, 4, 8, 16 parts. In Figure 58b, the mesh where the subareas are divided into 4 parts is depicted.

Figure 59 – Irregular polygonal panel: subdivision in areas and singular point

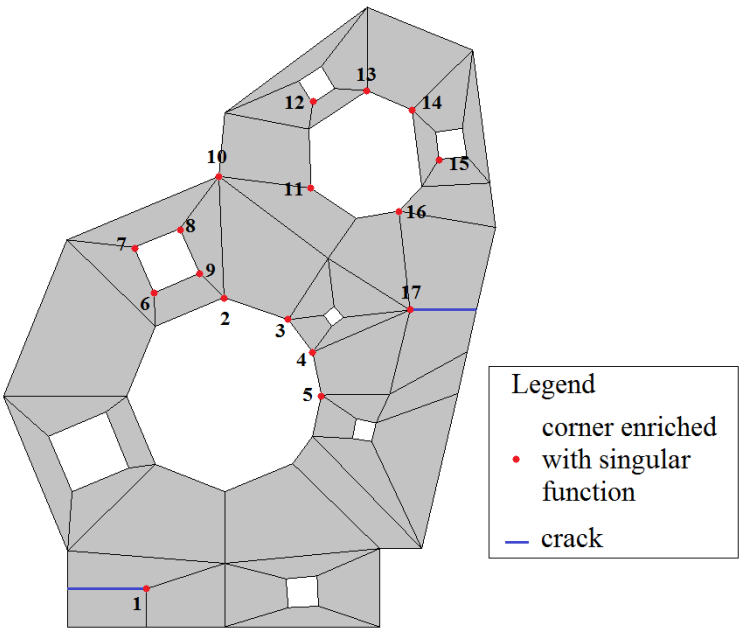

Shifted incomplete and complete second degree polynomials combined with singular functions were considered for enrichment. The polynomial was imposed to the whole set of nodes. The singular enrichment was applied at the corners and crack tips highlighted in Figure 59, following the layer-schemes 0 and 1, as described in the previous examples.

The corners where the singular function was applied were selected by analyzing the stress distribution shown by the reference numerical solution. In this solution, the 17 corners highlighted in Figure 59 presented a more significant stress concentration.

Table 9 lists the parameters adopted and the singular functions used in each of the selected corners.

Table 9 – λ parameter and singular function for each corner

Corner number	λ	Singular function	Corner number	λ	Singular function
1	0.5	$r^{\lambda}\cos(\lambda\theta)$	10	0.743723	$r^{\lambda}\cos(\lambda\theta)$
2	0.877278	$r^{\lambda}\sin(\lambda\theta)$	11	0.769407	$r^{\lambda}\cos(\lambda\theta)$
3	0.883286	$r^{\lambda}\sin(\lambda\theta)$	12	0.663369	$r^{\lambda}\cos(\lambda\theta)$
4	0.811627	$r^{\lambda}\sin(\lambda\theta)$	13	0.761295	$r^{\lambda}\cos(\lambda\theta)$
5	0.84071	$r^{\lambda}\sin(\lambda\theta)$	14	0.750657	$r^{\lambda}\cos(\lambda\theta)$
6	0.666667	$r^{\lambda}\cos(\lambda\theta)$	15	0.667065	$r^{\lambda}\cos(\lambda\theta)$
7	0.662808	$r^{\lambda}\cos(\lambda\theta)$	16	0.829467	$r^{\lambda}\cos(\lambda\theta)$
8	0.672313	$r^{\lambda}\cos(\lambda\theta)$	17	0.5	$r^{\lambda}\cos(\lambda\theta)$
9	0.664954	$r^{\lambda}\cos(\lambda\theta)$			

A comparison between the GFEM versions is presented next. The main aspects evaluated are the rate of convergence based on the relative errors in displacements and the SCN.

The reference solution u_{ref} needed for computing the relative error through expression (21) was obtained by a FEM analysis using a very refined structured mesh. In this mesh, the edges of the subareas were divided into 256 segments.

Relative errors in displacements computed using the ℓ_2 norm for combined enrichment cases are presented in log x log scale graphs, as shown in Figures 60 and 61.

Figure 60 – Irregular polygonal panel: h-convergence for incomplete polynomial and singular layer 0

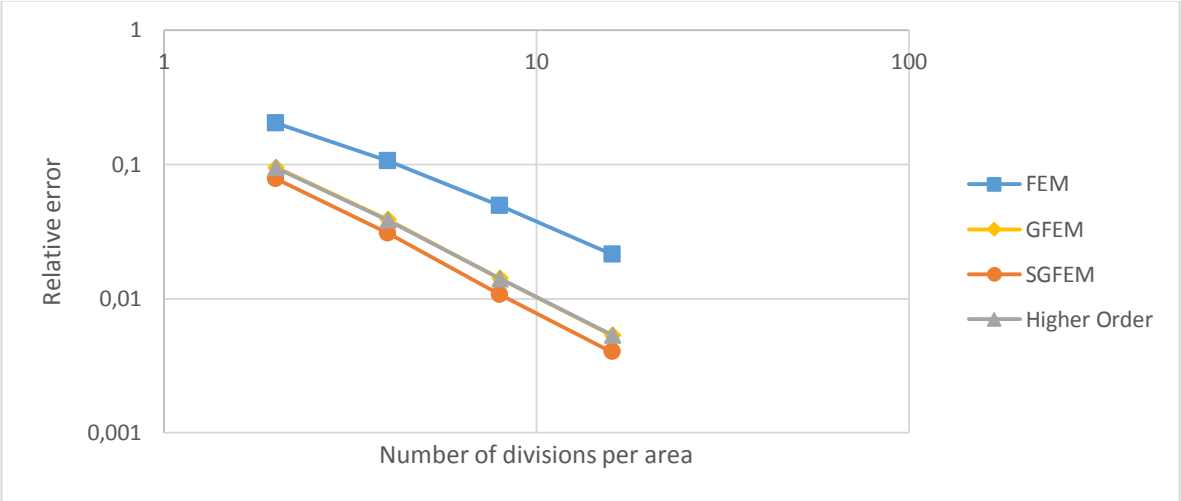

Figure 61 – Irregular polygonal panel: h-convergence for incomplete polynomial and singular layer 1

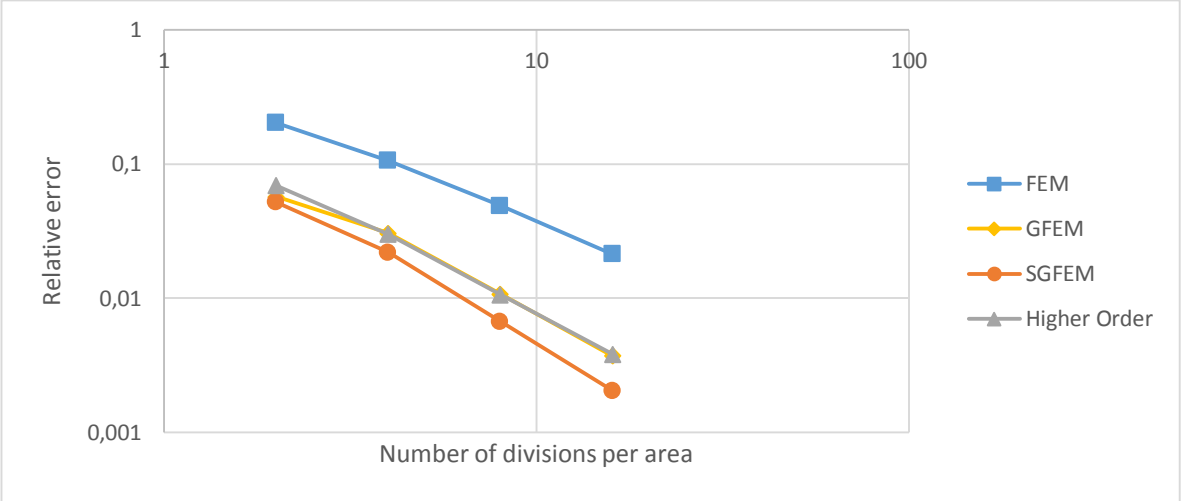

This problem involving multiples reentrant corners and two edge cracks induces heavy stress singularity in more than one place. Nevertheless, it can be observed that the GFEM version converges faster than FEM. Although a large number of blending elements can be found in this example, the h-convergence ratio is well-behaved.

In Figure 62, the SCN related curves are shown. For the incomplete case, the SCN for SGFEM and higher order SGFEM almost have the same order as the FEM. The GFEM curve presents a higher order for the SCN, but it is still acceptable. Comparatively, the benefits of using SGFEM and higher order version can easily be concluded.

Figure 62 – Irregular polygonal panel: SCN for incomplete polynomial and singular layer 0

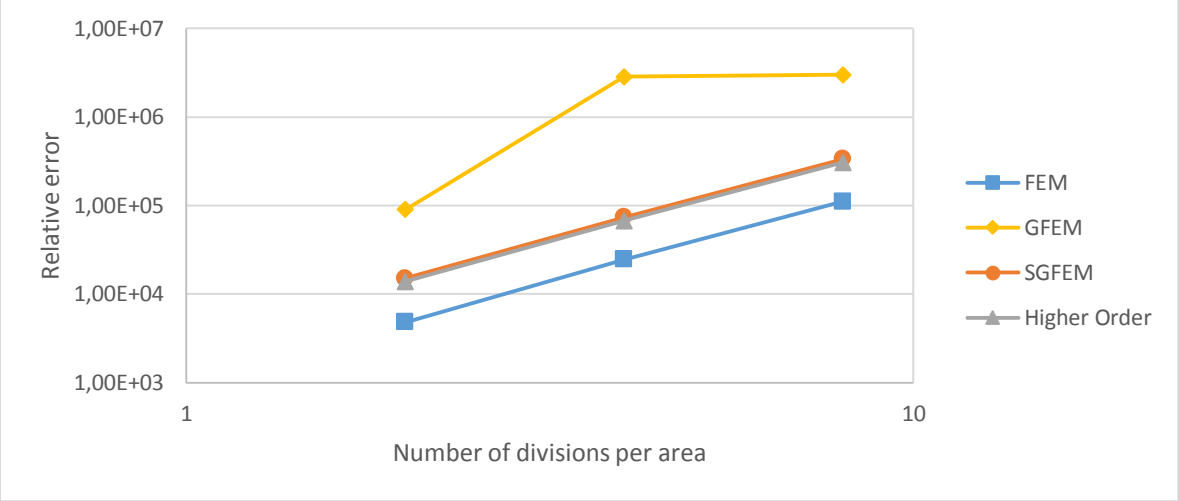

When considering complete polynomial enrichment combined with singular enrichment for layer-scheme 1, the approximate solution improves compared to FEM, in the way the relative error for a same mesh is smaller, as shown in Figure 63.

In terms of h-convergence, the SGFEM shows to be the best among the GFEM versions discussed. However, the complete polynomial contains a parcel which makes the resulting shape functions linearly dependent. Consequently, the SCN becomes high enough to make the solution less reliable, Table 10.

Figure 63 – Irregular polygonal panel: h-convergence for complete polynomial and singular layer 1

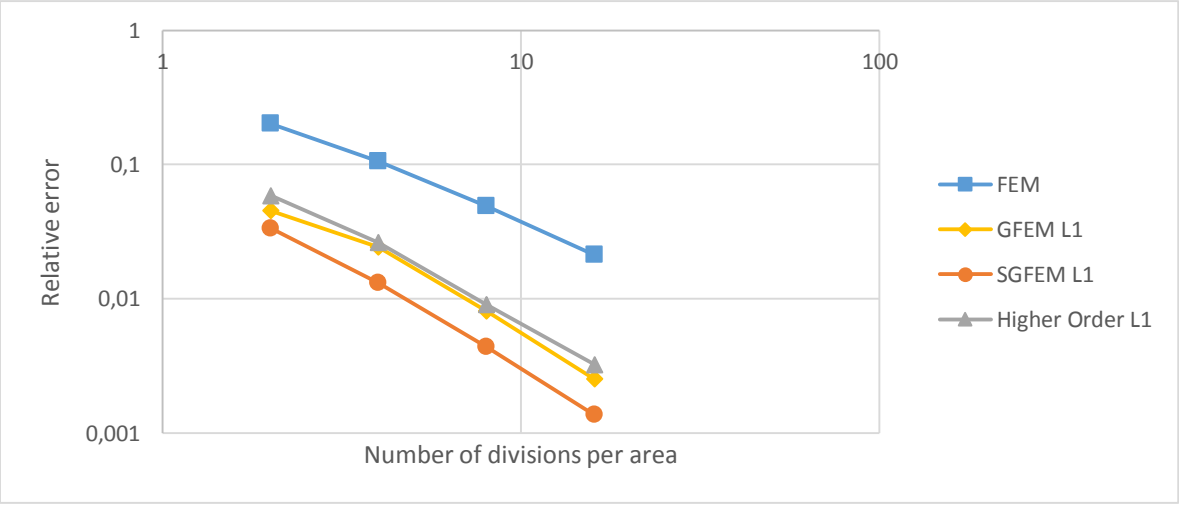

Despite the higher level of the relative error of the GFEM with respect to the SGFEM, its low SCN makes the higher order SGFEM a more reliable method.

Table 10 – Irregular polygonal: SCN for complete polynomial and singular layer 1

Number of divisions per area	FEM	GFEM	SGFEM	Higher Order $\sigma = 0.1$
2	4.81E+03	1.71146E+16	1.19674E+16	1.86E+04
4	2.46E+04	5.9114E+15	1.13896E+16	9.29E+04
8	1.11E+05	1.2702E+16	5.55485E+16	4.17E+05

Once again, the higher order benefits from the mesh refinement as shown in Figure 64.

Figure 64 – Irregular polygonal panel: Effect of mesh refinement.

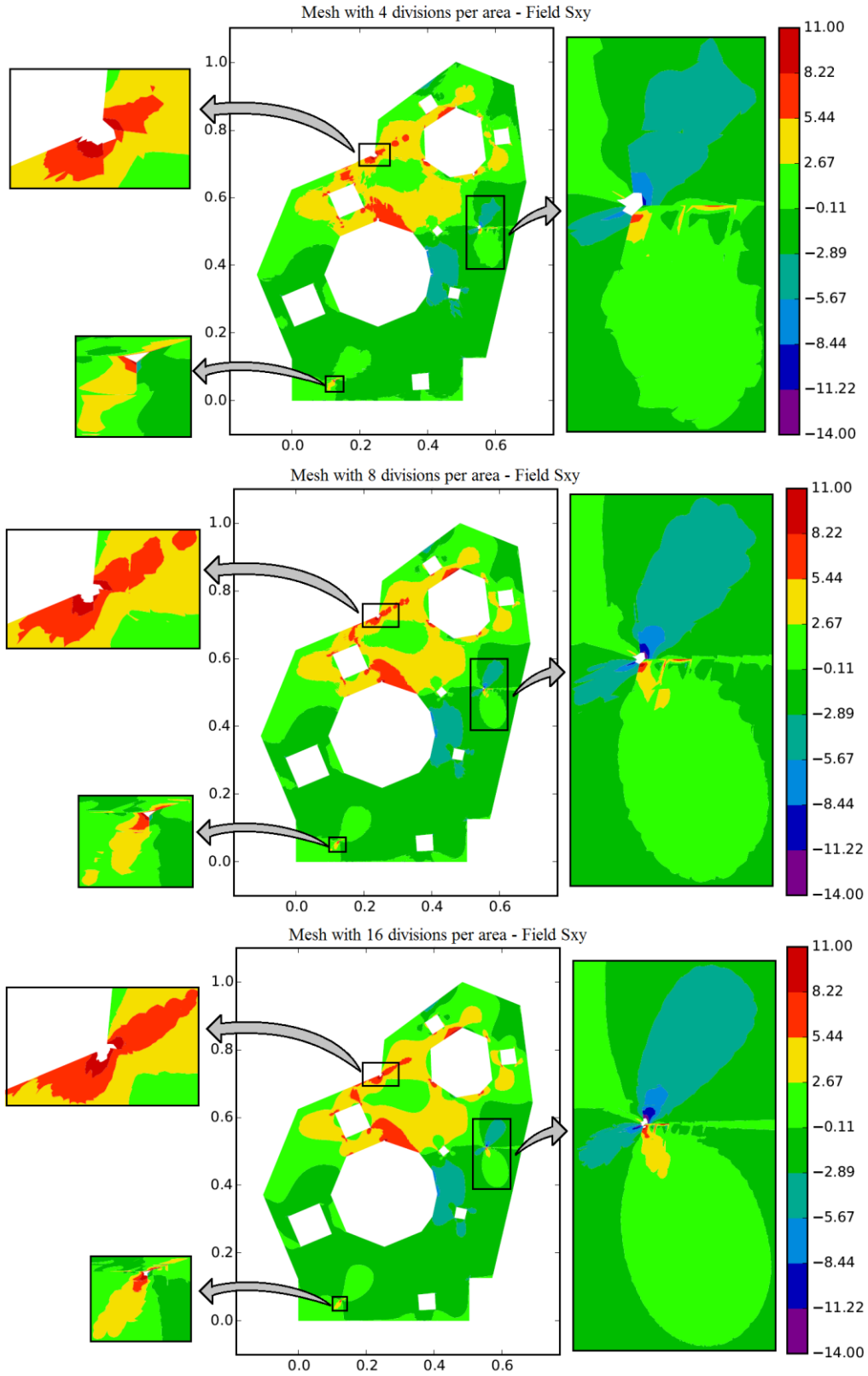

8 CONCLUSION

In this research, new versions of the generalized finite element method were numerically tested through a combination of polynomial and singular enrichment functions for increasing the approximation space. The new versions hereby considered were originally conceived to overcome two major drawbacks that may significantly influence the convergence and stability of the GFEM. They are the problem of ill-conditioning caused by linear dependencies induced into the solving system through the adopted enrichment and the appearance of the blending elements when the enrichment is restricted to a part of the domain.

Three examples allowing the possibility of local enrichment and consisting of structural panels were considered for performing linear 2-D analysis. The basic geometric features of the examples herein described were the existence of reentrant corners and cracks, both inducing stress concentrations restricted to the regions around it. Therefore, in order to capture such localized effects, the singular function enrichment was explored only in a neighboring region from those points. Polynomial enrichments were used to capture the smooth parts of the solutions.

In the stable GFEM version, a modification of the enrichment function is proposed aiming to guarantee stability comparable to the FEM solving linear system. Nevertheless, as concluded from the examples, linear dependencies still remain when the enrichment is a complete polynomial, therefore making the solution unreliable. Hence, as already observed in the original formulation, it was confirmed that the above mentioned modification is not a sufficient condition for stability.

Aiming to further investigate the SCN issue, now considering that high values for it cannot be completely avoided in the SGFEM, an improved version of the SGFEM was tested numerically. Once again, the numerical analysis was over the 2-D panels. In conclusion, the higher order SGFEM fulfilled what was proposed in its formulation, i.e. the scaled condition number comparable to the FEM values. Therefore, taking the low levels of scaled condition number as the criterion for comparison, this method appears to be more reliable than the GFEM and SGFEM. Despite this good feature, it is important to point out that taking the same mesh into consideration, the higher order SGFEM provides results including a larger error margin when compared mainly with the SGFEM results.

Finally, throughout the tested examples, it was also observed that the blending elements for the case of singular enrichment do not cause significant harmful effects to the rate of convergence.

REFERENCES

Babuška, I.; Osborn, J. E. **Generalized finite element methods**: their performance and their relation to mixed methods. SIAM Journal on Numerical Analysis, 1983, vol. 20, no. 3, p. 510-536.

Babuška, I.; Banerjee, U. **Stable generalized finite element method (SGFEM)**. Computer Methods in Applied Mechanics and Engineering, 2012, 201-204, p. 91-111.

Babuška, I.; Caloz, G.; Osborn, J. E. **Special Finite Element Methods for a Class of Second Order Elliptic Problems with Rough Coefficients**. SIAM Journal on Numerical Analysis, 1994, vol. 31, no. 4, p. 945-981.

Daux, C.; Moës, N.; Dolbow, J.; Sukumar, N.; Belytschko, T. **Arbitrary branched and intersecting cracks with the extended finite element method**. International Journal for Numerical Methods in Engineering 2000, 48, p. 1741–1760.

Dolbow, J.; Moës, N.; Belytschko, T. **Discontinuous enrichment in finite elements with a partition of unity method**. Finite Elements in Analysis and Design, 2000, 36, p. 235 –260.

Piedade Neto, D.; Ferreira, M. D. C.; Proença, S. P. B. **An Object-Oriented class design for the Generalized Finite Element Method programming**. Latin American Journal of Solids and Structures, 2013, vol.10, p.1267-1291.

Duarte, C. A. **The hp Cloud Method**. PhD dissertation, The University of Texas at Austin, Austin, TX, USA, 1996.

Duarte, C.A.; Babuška, I.; Oden, J.T. **Generalized finite element method for three-dimensional structural mechanical problems**. Computer & Structures, 2000, **77**, p. 215-232.

Duarte, C. A.; Reno, L. G.; Simone, A. **A high-order generalized FEM for through-the thickness branched cracks**. International Journal for Numerical Methods in Engineering, 2007, 72, p. 325–351.

Fries, T-P. **A corrected XFEM approximation without problems in blending elements**. International Journal for Numerical Methods in Engineering, 2008, v. 75, p. 503-532.

Fries, T-P.; Belytschko, T. **The generalized/extended finite element method:** An overview of the method and its applications. International Journal for Numerical Methods in Engineering, 2010, v. 84, p. 253-304.

Griebel, M.; Schweitzer, M.A. **A particle-partition of unity method,** Part II: efficient cover construction and reliable integration. SIAM J. Sci. Comput, 2002, 23(5), p. 1655-1682.

Gupta, V.; Duarte, C. A.; Babuška, I.; Banerjee, U. **Stable GFEM (SGFEM):** Improved conditioning and accuracy of GFEM/XFEM for three-dimensional fracture mechanics. Computer Methods in Applied Mechanics and Engineering, 2015, 289, p. 355-386

Gupta, V.; Kim, D.; Duarte, A. **Analysis and improvements of global–local enrichments for the Generalized Finite Element Method**. Computer Methods in Applied Mechanics and Engineering, 2012, 245–246, p. 47–62.

Ji, H.; Dolbow, J. **On strategies for enforcing interfacial constraints and evaluating jump conditions with the extended finite element method**. International Journal for Numerical Methods in Engineering 2004, 61, p. 2508 –2535.

Lins, R. M. **A posteriori error estimations for the generalized finite element method and modified versions**. Tese (doutorado), Universidade de São Paulo, 2015.

Melenk, J. M.; Babuška, I. **The partition of unity finite element method**: Basic theory and applications. Computer Methods in Applied Mechanics and Engineering, 1996, 139, p. 289-314.

Moës, N.; Dolbow, J.; Belytschko, T. **A finite element method for crack growth without remeshing**. International Journal for Numerical Methods in Engineering, 1999, 46(1), p. 131–150.

Simone, A.; Duarte, C. A.; Van der Giessen, E. **A Generalized Finite Element Method for polycrystals with discontinuous grain boundaries**. International Journal for Numerical Methods in Engineering, 2006, 67, p. 1122–1145.

Stroboulis, T.; Babuška, I.; Copps, K. **The design and analysis of the generalized finite element method**. Computer Methods in Applied Mechanics and Engineering, 2000, 181, p. 43-69.

Strouboulis, T.; Copps, K.; Babuška, I. **The generalized finite element method**. Computer Methods in Applied Mechanics and Engineering, 2001, 190, p. 289-314.

Sukumar, N.; Srolovitz, D. J.; Baker, T. J.; Prévost, J. H. **Brittle fracture in polycrystalline microstructures with the extended finite element method**. International Journal for Numerical Methods in Engineering, 2003, 56, p. 2015 –2037.

Szabo, B.A.; Babuška, I. **Finite Element Analysis**. Wiley, New York, 1991, p. 169±173.

Torre, D. A. F.; Barcellos, C. S.; Mendonça, P. T. **Effects of the smoothness of partitions of unity on the quality of representation of singular enrichments for GFEM/XFEM stress approximations around brittle cracks**. Computer Methods in Applied Mechanics and Engineering, 2015, 283, p. 243-279.

Zhang, Q.; Banerjee, U.; Babuška, I. **Higher order stable generalized finite element method**. Numerische Mathematik, 2014, 128: 1-29, DOI:10.1007/s00211-014-0609-1.